12-2011

Atlantic Multidecadal Oscillation-Forced Regional Summertime Precipitation Variations in the Central United States

Michael C. Veres
University of Nebraska-Lincoln, michael.veres@yahoo.com

ATLANTIC MULTIDECADAL OSCILLATION-FORCED REGIONAL SUMMERTIME PRECIPITATION VARIATIONS IN THE CENTRAL UNITED STATES

by

Michael C. Veres

A THESIS

Presented to the Faculty of

The Graduate College at the University of Nebraska

In Partial Fulfillment of Requirements

For the Degree of Master of Science

Major: Earth and Atmospheric Sciences

Under the Supervision of Professor Qi Hu

Lincoln, Nebraska

December, 2011

ATLANTIC MULTIDECADAL OSCILLATION-FORCED REGIONAL SUMMERTIME PRECIPITATION VARIATIONS IN THE CENTRAL UNITED STATES

Michael C. Veres, M.S.

University of Nebraska, 2011

Advisor: Qi Hu

The purpose of this research is to identify the regional mechanisms by which the Atlantic Multidecadal Oscillation (AMO) influences summer (June-August) precipitation in the central U.S. This was accomplished by running two different sets of simulations using the Weather Research and Forecasting (WRF) regional climate model, one forced by observations and the other forced only by variations in the AMO as obtained via a global climate model (GCM). The results reveal a complex set of mechanisms active in the lower and middle troposphere by which the AMO influences summer circulation and precipitation in the central U.S. During the cold phase of the AMO, much of the central U.S. experiences increased lower tropospheric pressure and precipitation. However, small-scale variability in the pressure increase results in an overall weakening of the pressure gradient, with the greatest reduction occurring in the north-central U.S. This process results in a buildup in the central U.S. of moisture in the lower atmosphere. Additionally, the increased pressure redirects the flow near 700hPa to reduce the moisture contribution from the Gulf of Mexico, producing a more potentially unstable lower atmosphere during the cold phase in which moist air is capped by overlying dry air.

In the middle troposphere (500hPa), the increased precipitation is largely supported by increased positive relative vorticity. This increase is produced by cyclonic circulation and effective depth (isentropic thickness) anomalies. Anomalous convergence in the mid- to upper troposphere in the central U.S. appears to be the source for the stretching. The positive relative vorticity anomalies during the cold phase produce favorable conditions for baroclinic development and when combined with the potentially unstable atmospheric moisture profile, produce conditions more favorable for increased precipitation.

Acknowledgements

I would like to thank my thesis advisor, Dr. Qi Hu for providing guidance and inspiration for this research. Without him, this research would not have been possible. I would also like to thank Dr. Robert Oglesby and Dr. Song Feng, whose presence on my committee provided a wealth of knowledge and experience from which I was able to draw from. Finally, I would like to thank Cindy Hays, whose understanding of WRF and willingness to provide guidance made learning how to use WRF significantly easier. I would like to acknowledge that this research has been supported by NOAA grant NA09OAR4310188 and that the WRF model simulations were only possible with the support of the University of Nebraska-Lincoln computing facility.

Contents

Table of Figures

Chapter 1

Introduction

In the central United States (U.S.), summer precipitation anomalies have a considerable impact on agricultural production, the environment and society by damaging floods or straining water supplies and enhancing the risk of wildfires during drought. It would be possible to mitigate some of the consequences of the precipitation anomalies if they can be better understood and predicted accurately. To do this requires a more extensive understanding of the physical processes causing the development of the anomalous precipitation. To understand the processes in a region, large scale and regional scale (i.e., tens to hundreds of kilometers) circulations must be examined. In this study, it is the regional scale processes that will be investigated.

The low-level moist southerly flow from the Gulf of Mexico is a significant contributor to summertime moisture and precipitation in the central U.S. (e.g., Rasmusson 1967; Arritt et al. 1997; Mo et al. 2009). As the southerly flow is concentrated in a channel from the Gulf of Mexcio to the central and northern Great Plains, it is frequently referred to as the Great Plains Low Level Jet (LLJ; e.g. Bonner 1968). It has been shown that the frequency of a strong LLJ is directly related to the occurrence of increased precipitation in the central U.S. (Bell et al. 1995; Arritt et al. 1997). The mean location of the LLJ and the precipitation related to it also change position during the summer. Higgins et al. (1997) found that the LLJ and the precipitation induced by it are found in the northern U.S. during May and then transition

toward the southeast U.S. during the summer. The location of the northern section of the LLJ is important as Tuttle and Davis (2006) found that the exit region of the LLJ is a favorable location for convective development. Variations in the position or intensity of the LLJ can modify the distribution and amount of summertime precipitation in the central and eastern U.S.

The intensity and position of the upper level (200hPa-300hPa) westerly jet is also recognized and frequently identified as having strong influence on central U.S. precipitation. During the 1993 floods in the central U.S. and the Midwest, the jet stream was found to be stronger than normal and shifted toward the south from its climatological position (Bell and Janowiak 1995; Trenberth and Guillemot 1996; Mo et al. 1997). The southerly shift of the stronger jet displaced the seasonal storm track to the south, keeping it over the affected regions (Trenberth and Guillemot 1996). The shift in the storm track also made it easier for synoptic systems to access moisture from the Gulf of Mexico, further contributing to the increase in precipitation. Trenberth and Guillemot (1996) also identified an inverse process during the strong drought of 1988. The jet stream and storm track retreated to the north of its climatological position, separating the storms from the critical supply of moisture from the south and limiting the development of disturbances and precipitation in the central U.S.

Related to the upper level jet stream variation, Bell and Janowiak (1995) identified anomalistic patterns of upper level relative vorticity as contributing to the precipitation anomalies during the 1988 drought and 1993 floods. During the 1993 floods, there was increased relative vorticity over the northwestern U.S. which was then

advected over the central U.S. and Midwest. Analysis of the atmosphere during high rainfall synoptic events for 1993 by Anderson and Arritt (1998) indicates that positive relative vorticity occurs in similar locations in the lower to mid-troposphere as well. Positive relative vorticity is an important component to the development of atmospheric disturbances, as it can help induce the circulations needed for baroclinic instability and the development of synoptic systems. On the other hand, in the 1988 droughts, the central U.S. and Midwest were under a broad region of negative relative vorticity, which limited the capacity for baroclinic development. Similar to the vorticity anomalies, Bell and Janowiak (1995) also found differences in the upper level divergence during the 1988 drought and 1993 floods. During the 1993 floods, much of the central U.S. and Midwest were under a broad region of upper level divergence (and negative vorticity). The upper level divergence and compensating low level convergence would have intensified and sustained any synoptic systems entering the central U.S. and precipitation. In contrast, the central U.S. had extensive upper level convergence and low level divergence anomalies during the 1988 drought. The subsidence motion associated with these divergence anomalies would have suppressed the development of synoptic systems and contributed to the sustained drought conditions.

The precipitation anomalies in the central U.S. are not independent of those that occur in surrounding areas. Mo et al. (1997) found that there is an inverse relationship between the precipitation anomalies in the central and southeastern U.S. In periods with above average precipitation in the central U.S., there is usually below average precipitation in the southeast. This correlation between the precipitation anomalies have

been found at annual (Enfield et al. 2001) and seasonal (summer) timescales (Mo et al. 2009; Wang et al. 2010).

Some of these variations of the central U.S. summertime circulation and precipitation have been attributed to changes and fluctuations in the sea surface temperatures (SSTs) of the Pacific and Atlantic Oceans (e.g. Namias 1983; Hu and Feng 2007; Mo et al. 2009; Wang et al. 2010; Feng et al. 2010). Ting and Wang (1997) found that the Pacific SSTs have significant impact on precipitation in the U.S. They found that the North Pacific SSTs are strongly correlated with central U.S. precipitation and that a weaker correlation exists between the El Niño-Southern Oscillation (ENSO) and central U.S. precipitation. McCabe et al. (2004) suggested that another mode of North Pacific SST variability, the Pacific Decadal Oscillation (PDO) accounts for 24% of the drought variance in the central U.S.

McCabe et al. (2004) suggested that another oceanic cycle was statistically even more important to the occurrence of drought in the central U.S. They indicate that the Atlantic Multidecadal Oscillation (AMO; Kerr 2000) accounts for 28% of the drought variance in the central U.S. The AMO is a 60-80 year cycle in North Atlantic SSTs (Enfield et al. 2001). The AMO has no "neutral stage", but only a cold phase and a warm phase (below and above long-term average SSTs, respectively). The previous cold phase occurred in 1961-1990 and the current warm phase began in 1991. The AMO is most likely a result of variations in the thermohaline circulation (THC) or the Atlantic Meridional Overturning Circulation (A-MOC) in the Atlantic Ocean (Guan and Nigam, 2009). The THC (A-MOC) transports heat from the tropics toward the Arctic. In a cycle

that lasts approximately 70 years, the THC alternates between strong and weak transports of heat and salt (Delworth et al. 1993; Latif et al. 2004). This alternation in heat transport is responsible for the AMO SST anomalies (Guan and Nigam, 2009). Only a single complete cycle of the AMO has occurred during the observational era, but the AMO has been simulated in long-term model simulations (Knight et al. 2005) and inferred from climate reconstructions using tree-ring data (Gray et al. 2004; Feng et al. 2010).

The impact of North Atlantic SST forcing on the United States has been analyzed from using observed SST anomalies (e.g. Enfield et al. 2001; Schubert et al. 2004; Feng et al. 2010) as well as simulations using idealized SST anomalies (e.g., Hu and Feng 2007; Wang et al. 2008; Mo et al. 2009; Feng et al. 2010; Hu et al. 2011). The general consensus is that a warm North Atlantic Ocean (warm phase of the AMO) produces below average summertime precipitation in the central U.S. (Hu and Feng 2008; Wang et al. 2008; Wang et al. 2010; Feng et al. 2010; Hu et al. 2011). Schubert et al. (2004) attributes the 1930s "Dust Bowl" era drought to warmer North Atlantic SSTs. In general, the warm SSTs weaken the North Atlantic Subtropical High Pressure (NASH) and modify the LLJ in the central U.S. on the western flank of NASH (Wang et al. 2008; Feng et al. 2008. 2010; Hu et al. 2011). During periods of colder North Atlantic SSTs, NASH intensifies (Wang et al. 2010, Hu et al. 2011), resulting in increased moisture flow into the central U.S. As a result, summer precipitation in the central U.S. is generally found to be above average during the cold phase of the AMO (Sutton and Hodson 2005; Hu and Feng 2008; Mo et al. 2009; Feng et al. 2010; Wang et al. 2010; Hu et al. 2011).

There is no complete agreement as to the importance of the AMO as a primary forcing for precipitation anomalies in the U.S. McCabe et al. (2004) indicates that the AMO contributes 28% to the drought variance in the central U.S., compared to the 24% attributed to the PDO. Hu and Feng (2008) showed that the AMO has strongly affected the summertime precipitation in the central and western U.S. However, Mo et al. (2009) places the AMO in a supportive role for producing droughts in the central U.S. They suggested that the AMO modulates the mechanisms produced by the Pacific SST anomalies rather than being a primary forcing. They concluded that the warm phase of the AMO consistently produces below average precipitation in the central U.S. only during La Niña. Similarly, the cold phase of the AMO only consistently produces above average precipitation during El Niño. In the other two potential scenarios, the correlation between the AMO and central U.S. precipitation is much weaker. These disagreements indicate that additional research is needed to better understand the AMO influence on climate in the central U.S.

A large part of the research on the AMO and its influence on precipitation has been done at the hemispheric or global scale. Not every process can be resolved and identified on that scale (e.g. Feng et al. 2008), however. This research intends to provide a better understanding of the AMO and central U.S. precipitation by investigating the regional processes that may be forced by the AMO. To do this, a regional model is used to simulate the atmospheric circulation and precipitation during the summer months of June, July and August (JJA) during the cold and warm phases of the AMO. The use of a regional model allows for the simulation of small-scale processes over the central U.S.

that are not captured by coarser scale general circulation models. It is potentially through these small-scale processes that the large-scale forcings from the AMO are modulated in the central U.S. to produce the observed precipitation anomalies.

In the following two chapters (chapters 2 and 3), the data, methods and model used in this study are described in detail and the regional model is tested to evaluate its ability to simulate the key atmospheric phenomena in this study region. In Chapter 4, I will describe the regional model results and propose a mechanism to explain the regional processes by which the AMO influences central U.S. precipitation. Chapter 5 summarizes the proposed mechanism and explores how the understanding from this study contributes to the understanding of the AMO and central U.S. precipitation variations as well as proposing ways in which this study can be furthered.

Chapter 2

Data and Methods

2.1 Data

To determine the AMO effect on summer (June-July-August) precipitation variation in the central U.S., several different datasets are used. These data include observed monthly cumulative precipitation, as well as monthly mean and six-hourly observed atmospheric data.

The observed monthly precipitation data were provided by the Global Precipitation Climatology Centre (GPCC; Beck et al. 2005; Rudolf and Schneider 2005; Rudolf et al. 2003, 2005) and were obtained from the National Oceanic and Atmospheric Administration (NOAA) Earth System Research Laboratory (ESRL) Physical Sciences Division (PSD) [available for download from the NOAA/ESRL/PSD at http://www.esrl.noaa.gov/psd/data/gridded/data.gpcc.html]. The GPCC data are global scale and several versions are available that vary in spatial and temporal scales. Data are monthly mean precipitation and are available at either 1° or 0.5° resolution. These data are available as a full data or monitored product that spans from 1951 to 2004 and a more restricted product that begins in 1986. The dataset selected for this research is the full data gridded dataset at 0.5° × 0.5° resolution, which is able to provide the highest resolution with the greatest span of available years.

Data from the National Center for Environmental Prediction (NCEP) and National Corporation for Atmospheric Research (NCAR) Reanalysis Project (hereafter Reanalysis;

Kistler et al. 2001; Kalnay et al. 1996), available from 1948 to present, were used for both the observed monthly means and as a source of six-hourly atmospheric data [available for download from http://dss.ucar.edu/]. The two datasets used were ds090.2 for the monthly mean geopotential heights and ds090.0 for the six-hourly atmospheric data and are globally gridded with resolutions of 2.5° × 2.5° for both datasets. The six hourly Reanalysis data contain over 80 atmospheric and surface variables on 17 pressure levels and can be analyzed directly or used as input data to drive an atmospheric model. The Reanalysis data are not observations per se, but are derived from observations (Kalnay et al. 1996). The data sources for the Reanalysis project vary globally, but over the United States, the Reanalysis project primarily uses the twice daily and spatially sparse observations provided by the National Weather Service (NWS) radiosonde network (Kalnay et al. 1996). A model is then used to interpolate these data to four times daily, filling in the spatial gaps in the data as well as interpolating the data to a uniform latitude and longitude grid. As such, the Reanalysis data are tightly constrained and serve as a proxy for observations and for simplicity, will be referred hereafter as observations. The monthly mean winds and geopotential heights are available as derived products from the Reanalysis project are simply the monthly averages of the winds and geopotential heights available in the six-hourly data. For this research, the mean monthly winds and geopotential heights are considered at three pressure levels; 850hPa, 500hPa and 300hPa.

The global model dataset used in this research is from the General Circulation Model (GCM) experiments performed by Hu et al. (2011). In these experiments, a GCM was run with constrained global sea surface temperatures (SSTs). The North Atlantic

Ocean had positive and negative SST anomalies (using the climatological average as a base) imposed upon it to simulate the Atlantic SSTs found during the cold and warm phases of the AMO. All other SSTs beyond the North Atlantic were maintained at their climatological values. The results presented in Hu et al. (2011) are based on the 20 years of model integration after the first 7-yearr run for each phase of the AMO. These model runs were later extended to 50 years and provide a much larger dataset that was used in this research. The resolution of the data produced by Hu et al. (2011) is 2.8° × 2.8° and data are available at six-hourly intervals. Unlike the Reanalysis, where atmospheric variations can have multiple sources (i.e., forcings), the AMO-only forced data provide a comprehensive dataset of atmospheric variables that vary only by processes that are influenced by Atlantic SST related to the AMO.

2.2 Methods

The purpose of this study is to determine the mechanisms over the central U.S. which produce the observed (Hu and Feng 2008; Mo et al. 2009; Wang et al. 2010) and modeled (Hu et al. 2011) summer (JJA) precipitation anomalies that are forced by the AMO. The emphasis of this study is on the regional scale processes that contribute to the AMO-forced precipitation anomalies. To do this, the AMO-forced data from Hu et al. (2011) must be downscaled from the coarse 2.8° resolution to a much finer resolution that would allow for the study of regional and local scale circulations. Simple regridding of the data is not sufficient, as sub-grid point scale dynamical processes would still be unaccounted for. Thus, the AMO-forced data must be used as forcing for a regional

model so that the small scale processes can be modeled. For the regional model, version 3.1 of the Weather Research and Forecasting (WRF) Advanced Research WRF (ARW) core was used (Skamarock 2005). All model runs performed in this research used identical domains and model parameters. The model was run using the Noah Land-Surface and Monin- Obukhov surface physics options. For the cumulus physics parameterization, the Kain-Fritsch scheme was selected. Data were output at three hour intervals.

In order to describe the regional scale processes that influence JJA precipitation over the central U.S., two domains were used (Figure 2.1), an outer domain and a nested domain. The feedback option between the nested domain and its parent (outer domain) was not used. Thus the outer domain provided the forcing at the boundaries of the inner domain, but the inner domain did not influence the outer domain. In the early stages of this study, the feedback option was used and the result showed precipitation magnitudes that were much weaker than observed (when compared to mean precipitation magnitudes). As a result, the feedback was removed in the model to produce more realistic precipitation magnitudes.

The outer domain has a resolution of 48km and contains nearly all of North America. This domain extends from southern Mexico in the south (around 15-20°N) to northern Alaska and the Queen Elizabeth Islands in the north (around 65-75°N). The longitudinal boundaries of the outer domain vary widely as the native map projection for the domain is Lambert Conformal. In general, the western and eastern boundaries lay approximately 20° of longitude off the coasts of the Continental U.S. The primary

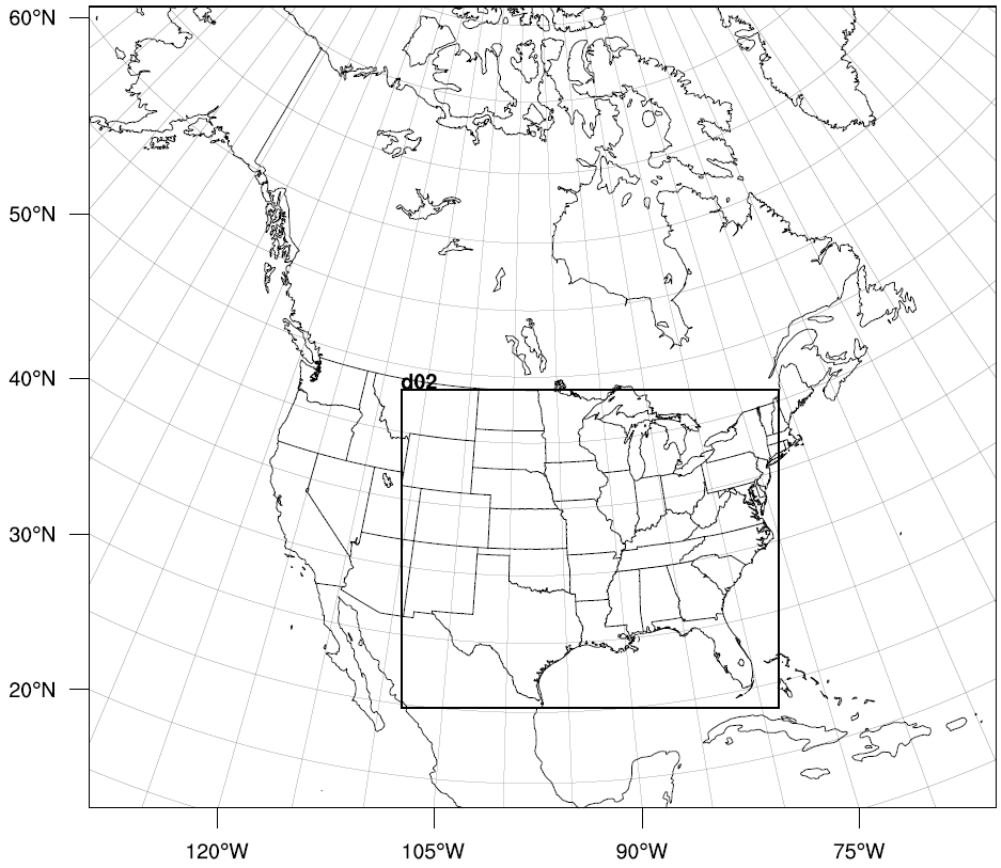

Figure 2.1 The two domains used in this study. The outer domain includes the entire image and the inner domain (d02) is bounded by the heavy black box.

purpose for using an outer domain of this size is to provide adequate distance between the boundaries of the two domains for effective downscaling of the coarse resolution input data. The large outer domain also allows for the model to have a greater freedom in developing the forcing used along the boundaries of the second domain.

The inner domain has a finer resolution of 12km, which allows for the development of small scale internal processes within the central U.S. The inner domain consists of nearly all of the Continental U.S. east of the Rocky Mountains, with only the omission of part of eastern New England. The southern boundary starts near 25°N latitude and includes the northern half of the Gulf of Mexico, while the northern boundary is approximately parallel to the U.S.-Canadian border in the western half of the domain and includes the far southern reaches of the Ontario and Quebec provinces of Canada in the eastern half of the domain. The western and eastern boundaries of the inner domain are approximately at 110°W longitude in the west and 70-78°W longitude along the Atlantic coast of the Continental U.S. in the east. The size and positioning of the inner domain were guided by previously described descriptions of large scale AMO-forced mechanisms and precipitation anomalies (e.g, Enfield et al. 2001) as well as computational limitations.

The importance of the moist southerly flow on central U.S. precipitation (e.g. Rasmusson 1967; Higgins et al. 1997) suggested the inclusion of the far southern U.S. and the northern Gulf of Mexico in the inner domain. Similarly, the frequent description in the literature of an anomalous precipitation dipole between the southeastern and central U.S. (Arritt et al. 1997; Mo et al. 2009; Wang et al. 2010) suggests that the process that

produces the observed precipitation anomalies in the central U.S. during the cold phase of the AMO may be related to the positive anomalies in the southeast during the warm phase. The northern and western boundaries were chosen such that the entire central U.S. was included within the high resolution domain. The domain used in this study produced a dataset that was near the limitations of available computational capabilities. Therefore, extension of the northern and western boundaries much beyond what was chosen would not be computationally feasible.

The inner domain used in this research has never been previously used in a regional modeling experiment. As such, it must be verified that the model with the specified domain-setting is capable of producing realistic atmospheric conditions. In order to validate the model and domain, the Reanalysis data were used to force WRF for five specified summers from each phase of the current AMO cycle, for a total of ten summer seasons. For the purposes of this experiment, the cold phase of the AMO was defined as 1961-1990 and the warm phase of the AMO was defined as 1991-2009. The regional model was initialized at 0000Z on 16 May of each year and was run until 0000Z of 1 September of the same year, with the first two weeks of each model run discarded as model spin-up. These results were then compared to observations to validate the model's accuracy. The modeled precipitation magnitudes and anomalies were compared to the observations to determine how effective the model is at reproducing the observed precipitation. The modeled winds and geopotential heights at 850hPa, 500hPa and 300hPa were compared to observations to determine how accurately the model is capable of simulating the lower, middle and upper atmospheric circulations, respectively. As

they are based on similar data, the comparison of the winds and the geopotential heights provides an indication as to the extent that the model modifies the data that force it.

For the validation, only ten years out of nearly fifty possible were used. To select the years used in the validation, it was assumed that the central U.S. would experience increased (decreased) precipitation during the cold (warm) phase of the AMO. There is a problem in selecting the years based solely on this assumption. It was shown in Ruiz-Barradas and Nigam (2005) that the correlation between observed precipitation and the Reanalysis precipitation is weak in the Great Plains. When compared to the observations, the Reanalysis data show a bias toward low summer precipitation during the cold phase (1960-1980) of the AMO and high summer precipitation during the warm phase (after 1990). To show this bias, the area averaged JJA precipitation for the Great Plains (using the same definition as in Ruiz-Barradas and Nigam, 2005; 35°-45°N, 90°-100°W) was calculated from the observations and the Reanalysis data (Figure 2.2). As with Ruiz-Barradas and Nigam (2005), the Reanalysis displays an upward trend with time in summertime precipitation, whereas the observations do not. In selecting the years used in this study, both the observations and the Reanalysis had to indicate increased (decreased) precipitation during the cold (warm) phase of the AMO. The magnitudes of the precipitation were not used in selecting the years; only the precipitation anomalies in both datasets, relative to the average of the years in the cold (warm) phase of the AMO were used. It was attempted to refrain from using years with a strong El Niño or La Niña, to attempt to minimize the influence of non-AMO forcings on the validation, but the low correlation between the observations and the Reanalysis required that the presence of

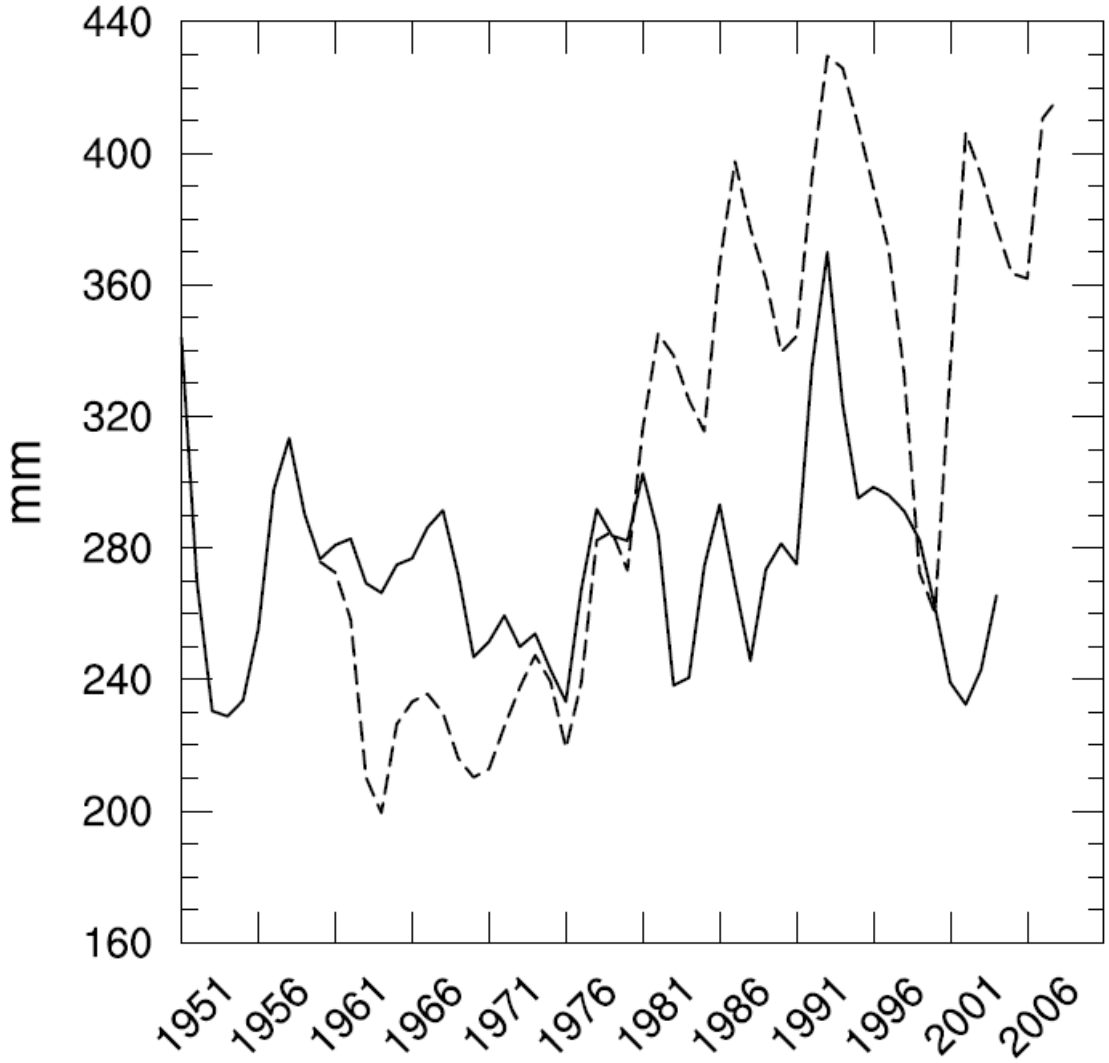

Figure 2.2 Observed JJA precipitation in the Great Plains (35-45°N, 90-100°W) from the GPCC (solid) and NCEP-NCAR Reanalysis (dashed) datasets. The values on the ordinate axis are accumulated JJA precipitation (in mm) and the abscissa shows years.

such an event not be a deciding factor. The years ultimately selected for the model validation are 1965, 1966, 1979, 1981 and 1986 for the cold phase and 1999-2003 for the warm phase of the AMO. These years generally have the best agreement in anomalies between the observations and the Reanalysis, while conforming to the assumed precipitation anomalies for each phase of the AMO. ENSO events were unable to be avoided and occur during 4-5 of the selected years (depending on the criteria used to define an ENSO event).

In addition to comparing the model output to the observations of the same years, the model output and observations described previously will be compared to the entire observational dataset for nearly a full cycle of the AMO (i.e. 1961-1990 for the cold phase and 1991-2008 for the warm phase). These comparisons serve two purposes. The first is to determine how accurately the model is able to simulate the observed conditions. The second is to determine how representative the selected years are for each phase of the AMO.

For the AMO-forced GCM output from Hu et al. (2011), the selection method was similar, though simpler than the previously described methodology. For these data, there were fifty years available for use from each phase of the AMO. The same number of years was used as in the Reanalysis; five years from the cold phase and five years for the warm phase of the AMO. The years were selected based on the same criteria used previously, that the central U.S. experiences increased (decreased) precipitation during the cold (warm) phase of the AMO. As these are purely simulated years, the years were selected solely on the magnitude of the summer precipitation anomalies. The five years

with the greatest precipitation from the cold phase simulations (model years 10, 21, 39, 41 and 45) and the five years with the lowest precipitation from the warm phase simulations (model years 7, 15, 27, 28 and 40) were selected.

All data (observed and simulated) used in this research were processed to produce seasonal (JJA) means and anomalies as well as averages of all ten years (i.e., the 10-year mean). For precipitation, the magnitudes are presented as precipitation accumulations. For all other parameters, the data were simply averaged. Averages include both mean and eddy terms, as all calculations (e.g., moisture flux) were performed at each individual model time-step prior to averaging.

Anomalies were calculated by subtracting 10-year mean from the 5-year mean for each phase of the AMO. This method for determining the anomalies results in mirror image anomalies are of equal magnitude and opposite sign. Since an equal number of years were used for both the cold and warm phases of the AMO, the 10-year mean is simply the average of the cold phase average and the warm phase average value. The following equations illustrate this,

$$X_{mean} = \frac{X_{cold} + X_{warm}}{2} \quad (1)$$

where, X is an arbitrary variable and its subscript indicates the 10-year mean or the 5-year mean for each phase. (2) and (3) below indicate the method used in calculating the anomalies in this study.

$$X_{cold\ (warm) phase\ anomaly} = X_{cold(warm)} - X_{mean} \quad (2)$$

If (2) is combined with (1), as shown in (3), it is apparent that the anomalies for each phase must be of equal magnitude and opposite sign and there are an equal number of years for each phase of the AMO;

$$X_{mean} = \frac{X_{cold\ phase\ anomaly} + X_{warm\ phase\ anomaly} + 2X_{mean}}{2} \quad (3)$$

This is only true for the cases when there are an equal number of years used for each phase of the AMO. An unequal number of years would produce anomalies that are opposite in sign, but differ in magnitude. This is only important to this study in one case, when the observed anomalies for 1961-2009 are examined. In this case, the number of years used for the cold phase nearly outnumbers the years for the warm phase. Beyond this particular exception, the remainder of the anomalies presented in this research will be mirror images. As a result of this, many of the figures shown in this study will contain only one phase of the AMO or the other, except where noted.

Chapter 3

Model Validation

Prior to using the regional model (WRF) to examine the physical processes forced by the AMO, it must be determined whether the model is capable of simulating realistic patterns of atmospheric circulation and precipitation in the U.S. The results of the WRF simulations forced by the selected years of the Reanalysis data will be compared to observations to determine the accuracy of the simulated atmosphere for the cold and warm phases of the AMO. The 850hPa, 500hPa and 300hPa wind and geopotential height fields will be used to determine the model's ability to accurately replicate the atmospheric circulations used as forcing.

A comparison between the GPCC observed summer (JJA) precipitation averaged over the ten selected years (Figure 3.1a) and the WRF simulated precipitation for the same period forced by the Reanalysis data (Figure 3.1b) reveals that the model is capable of simulating the mean summer precipitation within the model domain. The model accurately depicts the pattern of zonal and meridional variations in precipitation throughout the central U.S. The largest magnitudes of precipitation in the northern U.S. occur in Minnesota and Wisconsin in both the observations and the model simulations. Further to the south, the model simulates somewhat lower precipitation in Iowa, compared to the observations. In Arkansas, the model partially captures the reduction in precipitation, relative to the areas around it. While precipitation magnitudes in the central U.S. are modeled accurately, the magnitudes in New England are greater than in

observations. The model also greatly overestimates the precipitation in the Appalachian Mountains. On average, the accuracy of the model in simulating the mean precipitation decreases in the eastern part of the model domain.

This study is primarily interested in the differences in precipitation between the cold and warm phases of the AMO. As such, the accurate simulation of the anomalies is of even greater importance than the mean conditions if the difference in processes between the phases is to be determined. The results show that the model is able to reasonably simulate the JJA precipitation anomalies between the two phases of the AMO, albeit the anomalies are less consistent than the means when comparing the simulations to observations for each phase of the AMO. Figures 3.2a and 3.2b show the observed and simulated cold phase precipitation anomalies for JJA. The overall pattern for both the observations and the model simulations shows above average precipitation in much of the central U.S. during the cold phase of the AMO. A small region of decreased precipitation occurs in southern Texas and a more extensive region with below average precipitation occurs along the U.S.-Canadian border. The model and observations differ most significantly in the Midwest and the southeastern U.S., with the model simulating a more extensive region of below average precipitation during the cold phase in the Midwest as well as displacing the negative precipitation anomalies in the southeastern U.S. toward Florida. In the Midwest, the negative precipitation anomalies extend further to the south in the simulations. Even with the more extensive negative anomalies, the overall pattern in the Midwest is still reasonably consistent with the observations. The

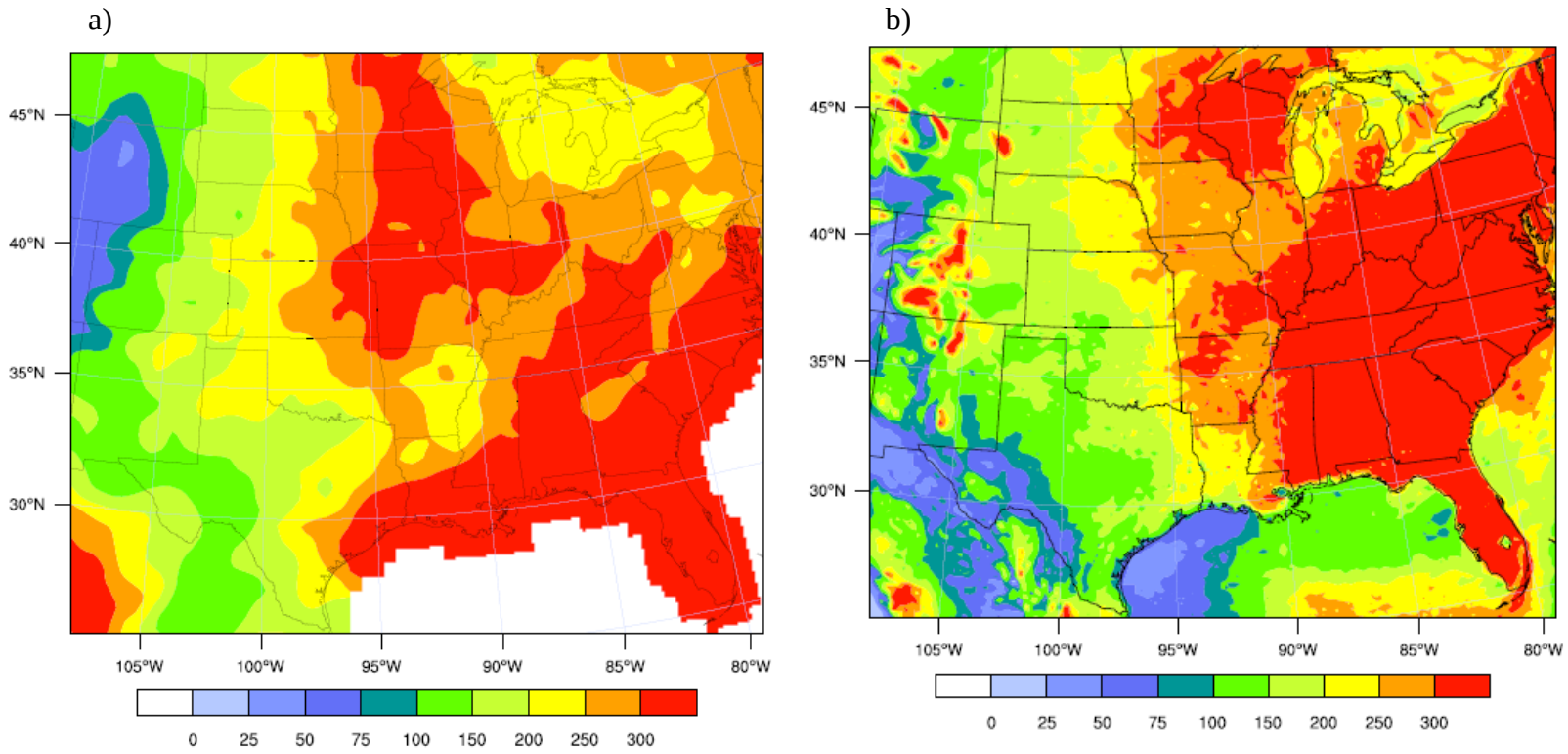

Figure 3.1 Mean (10-year) JJA accumulated precipitation for (a) observations and (b) Reanalysis-forced simulations. Units are in mm.

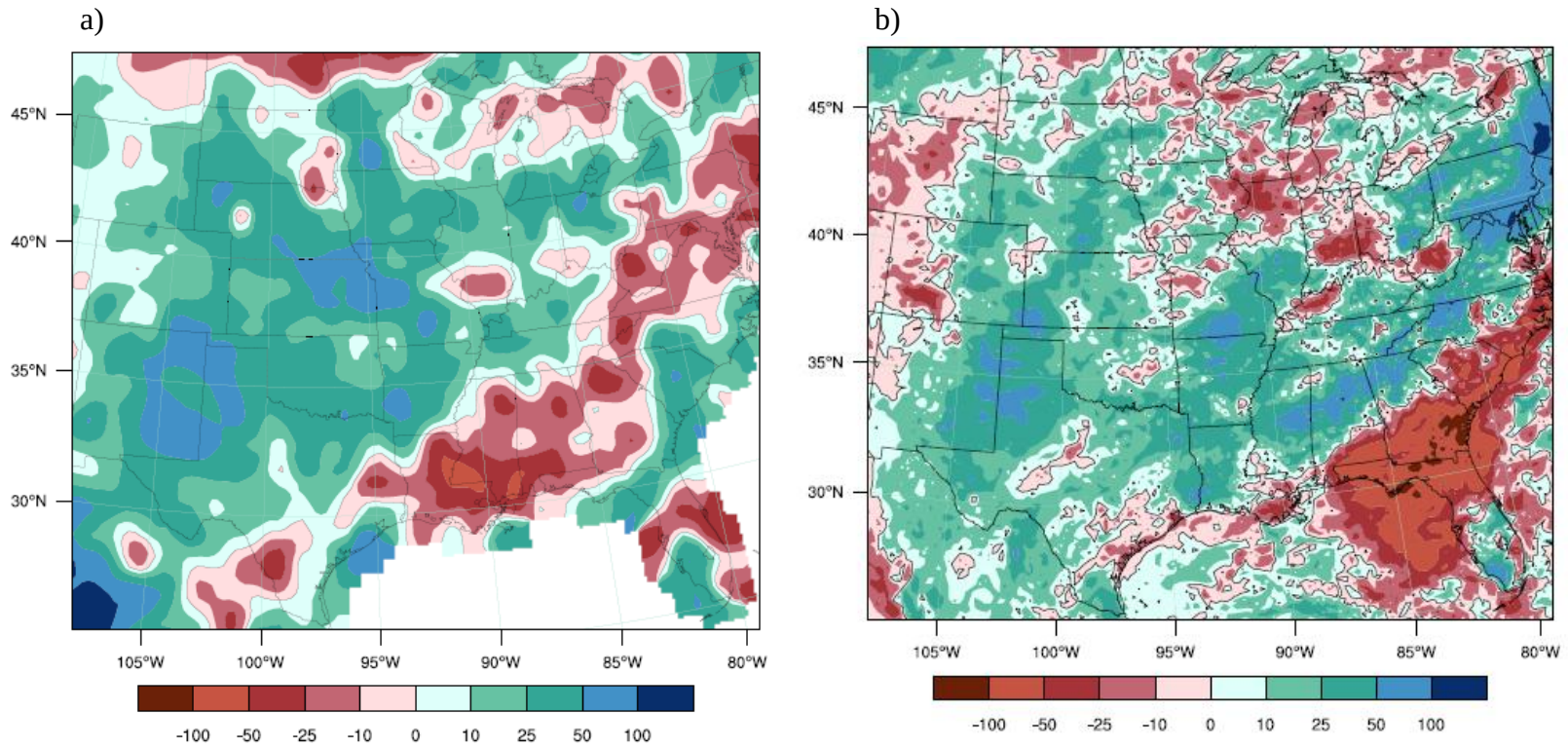

Figure 3.2 JJA cold phase accumulated precipitation anomalies for (a) observations and (b) Reanalysis-forced simulations. Units are in mm.

main difference between the observations and the simulations is that the model connects the negative anomalies in the Ohio River Valley and the Upper Midwest. In the southeast, there is an extensive region of negative precipitation anomalies oriented southwest to northeast in the observations and also the model runs. However, in the observations, the negative anomalies extend from Louisiana to New England and approximately follow the Appalachian Mountains. The simulated negative anomalies are closer to the Gulf of Mexico and Atlantic coasts and follow along the Atlantic coastline toward New England. The simulated anomalies over the Appalachian Mountains are actually the strongest positive anomalies produced. The presence of the negative anomalies in both the observations and the simulations indicates that the model is capable of reproducing the mechanism, but is unable to correctly place the mechanism to produce the anomalies in the correct location across the entire model domain. This is not of much concern, as the central U.S. and the Midwest are the principle areas of interest and the simulations of precipitation in those regions show consistency with the observations.

It is important that the model is capable of simulating not only precipitation, but also the atmospheric circulations that produced it. Comparison of the observed and modeled JJA 850hPa winds and geopotential heights (Figures 3.3a and 3.3b, respectively) averaged for the study years show that the model is able to replicate the 850hPa geopotential heights contained in the Reanalysis forcing. The model clearly captures the intrusion over the U.S. of the North Atlantic Subtropical High Pressure System (NASH). The high pressure has its greatest westward extent in the lower latitudes near 25-30°N. The isobars become oriented southwest to northeast over the central U.S. and then turn

eastward in the Midwest. However, the magnitudes of the geopotential heights across much of the U.S. are consistently 20-30m greater in the model than in the observations. The greater magnitudes are likely attributable to the model producing temperatures warmer than observed. The model increased the magnitudes of the geopotential heights across the U.S., but it did not have much of an impact on the spatial variability and gradient of the geopotential heights. The model was also capable of accurately simulating the 850hPa winds in the central U.S. The strong southerly flow into the central U.S. from the Gulf of Mexico shown in the observations also occurs in the simulations. A consistent pattern between the observed and simulated JJA winds and geopotential heights for the selected years as well as a minimal change in the pressure gradient indicates that the model was able to reasonably reproduce the observed mean conditions.

The model's ability to simulate the anomalies in the geopotential heights between the phases of the AMO is somewhat reduced in comparison to the mean geopotential heights for the ten study years. During the cold phase of the AMO, the observations (Figure 3.4a) show an anomalous wave pattern, with positive anomalies in the southeastern and north-central U.S. and an elongated region of negative anomalies in the Midwest. The model simulates a similar anomalous wave pattern during the cold phase of the AMO (Figure3.4b), but the magnitudes and positioning are different. The model produces decreased geopotential heights across the entire domain. In the simulations, there are weak pressure anomalies in the southeast and the anomalies amplify toward the northwest during the cold phase. The low pressure anomalies maximize in the Midwest

and then begin to weaken toward the north-central U.S. This pattern is analogous to the wave pattern present in the observations, where the highest pressures occur in the southeastern and north-central U.S. and the lowest pressures occur in the central U.S. and Midwest. As a result of the pressure anomaly minimum, part of the central U.S. has northerly wind anomalies during the cold phase. The observations place these anomalies in the west-central U.S. and the simulations place them in the east-central U.S.

The similar wave pattern and dissimilar magnitudes in the model results suggest that the model is capturing some, but not all, of the processes inducing the variations between the phases of the AMO. The anomalous wave pattern is arguably the more important of the two in influencing the low level dynamics, as it produces spatial variability in the pressure fields within a particular phase of the AMO. During the cold phase, the greater decrease in pressure in the Midwest and lesser decrease in the southeast would produce a change in the pressure gradient, thereby altering the low level wind fields. In contrast, the overall reduction of the pressure would not affect the pressure gradient or wind fields. Although there are differences, the overall similarities in anomaly patterns indicate the model appears to have reasonably captured the variations in the low level pressure fields.

Of potential concern is that when only the ten study years are examined, there are discrepancies between the observed geopotential heights shown in Figure 3.4a and previously published data on the effect of the AMO on the geopotential heights in the U.S. Previous studies (e.g. Wang et al. 2008; Hu et al. 2011) have indicated that relatively cold North Atlantic SSTs are correlated with positive low level pressure

anomalies over the southeastern U.S. that then weaken toward the northwest. If the entire range of Reanalysis data are used from 1961-2009 (hereafter full observations), then the 850hPa geopotential height anomalies for the cold phase of the AMO more closely resemble the expected pattern (Figure 3.5). During the cold phase, much of the U.S. east of the Rocky Mountains experiences increased low level pressures. The difference between the full and limited (i.e. the ten study years) observations are most apparent in the Midwest, where the limited observations (Figure 3.4a) have negative pressure anomalies and the full observations (Figure 3.5) have positive anomalies. As the years chosen for this study were selected based on their precipitation anomalies, this may suggest that the weakening of the low level pressures in the Midwest and the central U.S. may have a connection to the precipitation anomalies. This hypothesis will be explored in the next chapter using the AMO-forced model simulations. In the context of the model validation, the differences between the full and limited observations are less important, as the model reasonably simulated the atmospheric conditions when forced with the ten year dataset.

Comparisons of the wind and geopotential height fields between the observations and the model simulations reveal that the model is equally capable of simulating the basic atmospheric structure at 500hPa as well. The summertime ridge over the central U.S. and the trough over the eastern U.S. in the observations (Figure 3.6a) are clearly reproduced in the model simulations (Figure 3.6b). As with the model results at 850hPa, the pattern is reproduced accurately, but the model produces geopotential heights that are

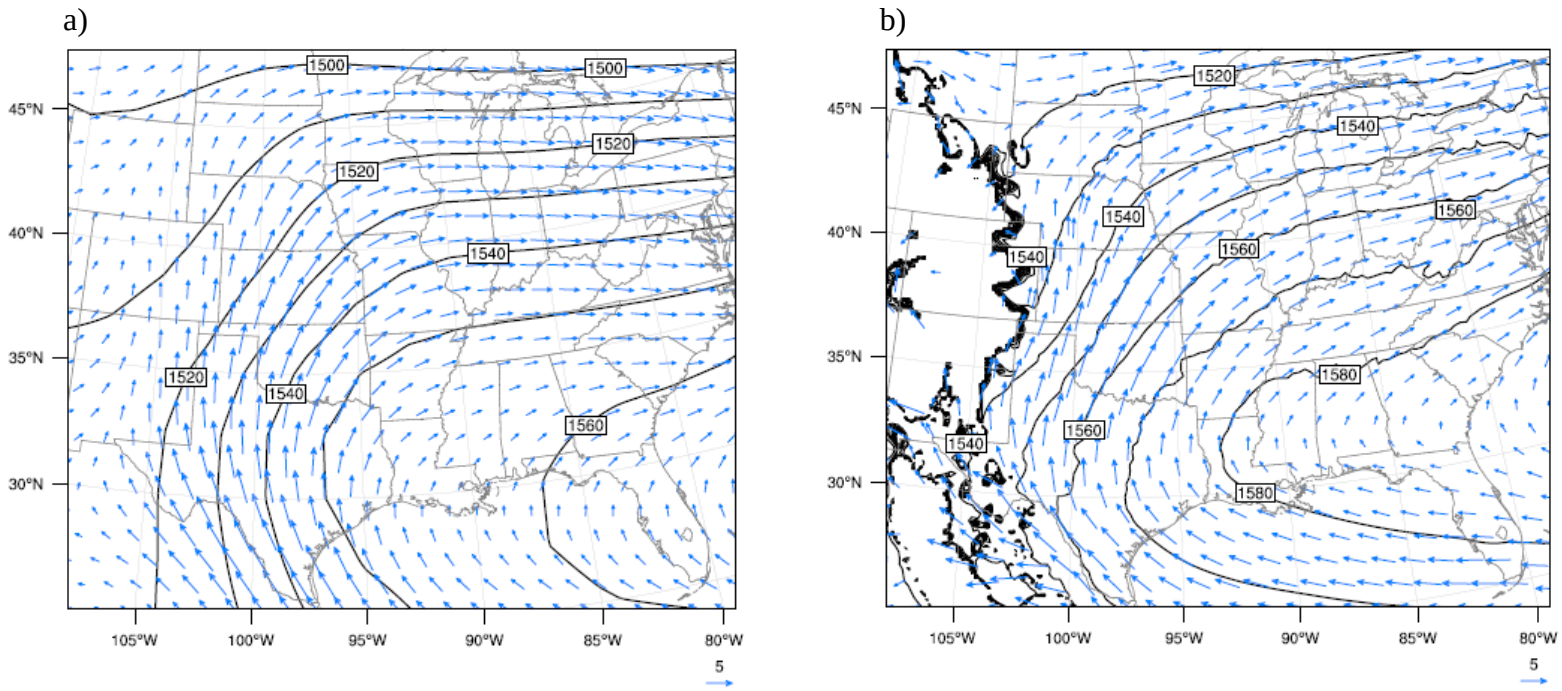

Figure 3.3 Mean (10-year) JJA 850hPa winds and geopotential heights for (a) the observations and (b) the Reanalysis-forced simulations. Units are in ms^{-1} (winds) and m (geopotential height). Reference vector is $5ms^{-1}$ and the contour interval is 10m with labels every 20m.

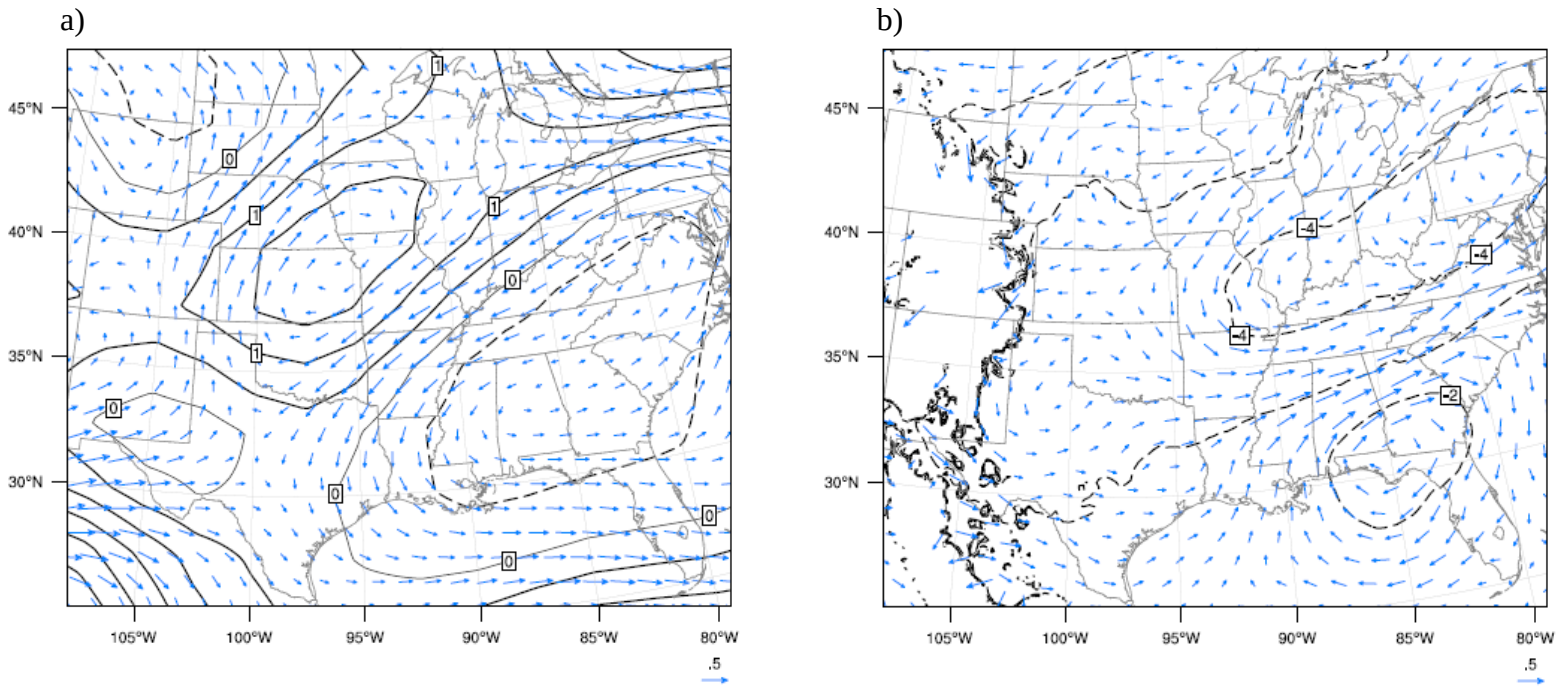

Figure 3.4 (a) Observed and (b) simulated JJA 850hPa wind and geopotential height anomalies for the cold phase of the AMO using the five study years for the cold phase (1965, 1966, 1979, 1981, 1986). Units are in ms^{-1} (winds) and m (geopotential height). Reference vector is $0.5ms^{-1}$ and the contour interval is 1m with labels every 2m. Solid (dashed) lines indicate positive (negative) contours.

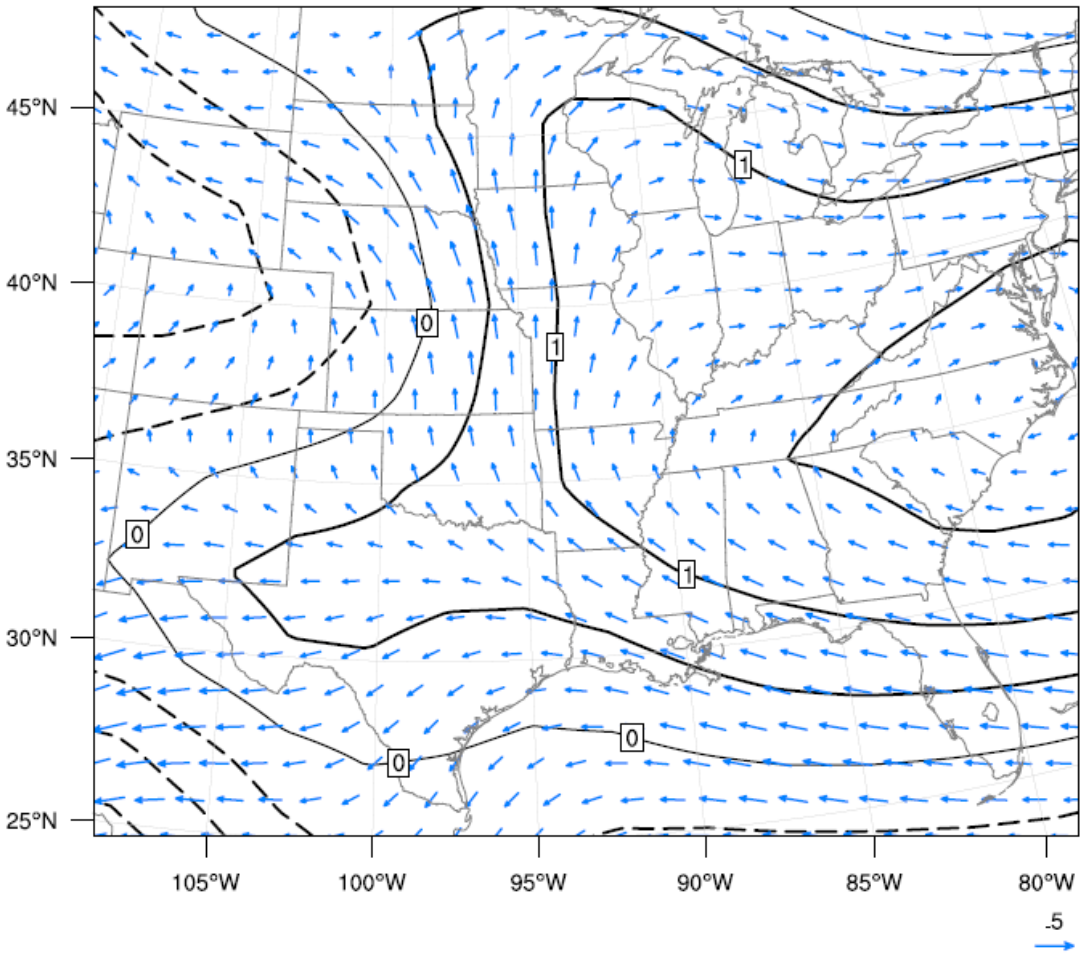

Figure 3.5 JJA 850hPa winds and geopotential height anomalies for the cold phase of the AMO using the full range of Reanalysis data (1961-1990 for the cold phase, 1990-2009 for the warm phase). Units are in ms^{-1} (winds) and m (geopotential height). Reference vector is $0.5ms^{-1}$ and the contour interval is 0.5m with labels every 1m. Solid (dashed) lines indicate positive (negative) contours.

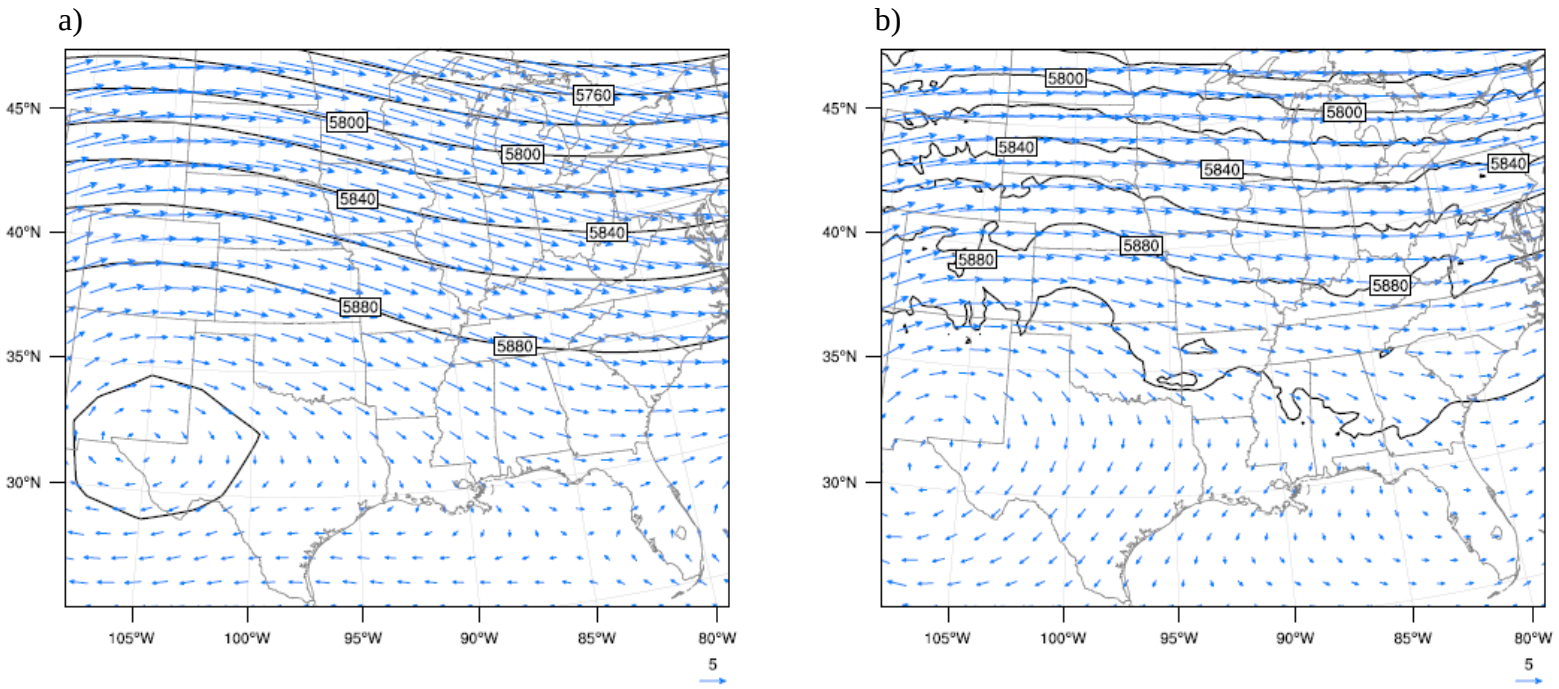

Figure 3.6 Mean (10-year) JJA 500hPa winds and geopotential heights for (a) the observations and (b) the Reanalysis-forced simulations. Units are in ms^{-1} (winds) and m (geopotential height). Reference vector is $5ms^{-1}$ and the contour interval is 10m with labels every 20m.

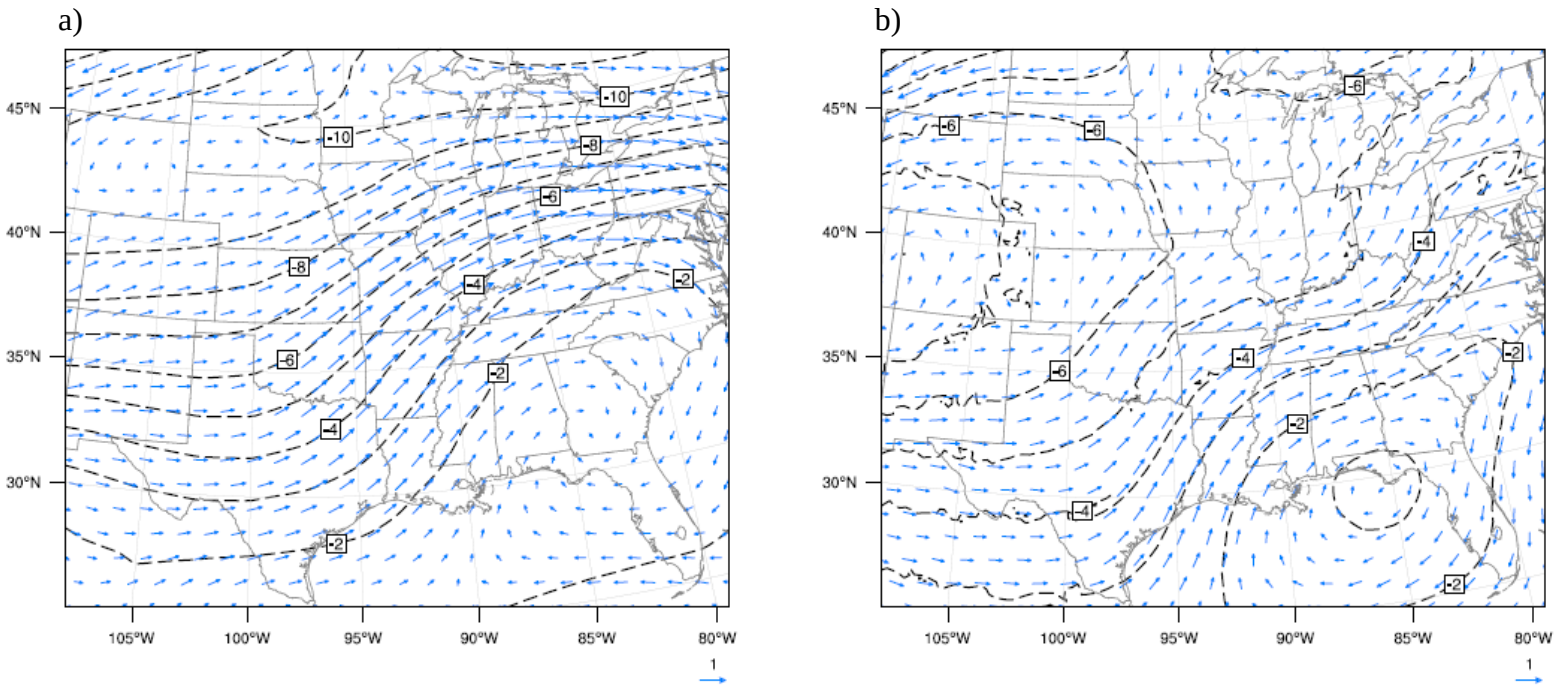

Figure 3.7 (a) Observed and (b) simulated JJA 500hPa wind and geopotential height anomalies for the cold phase of the AMO using the five selected years for the cold phase (1965, 1966, 1979, 1981, 1986). Units are in ms^{-1} (winds) and m (geopotential height). Reference vector is $1ms^{-1}$ and the contour interval is 1m with labels every 2m. Solid (dashed) lines indicate positive (negative) contours.

consistently about 20m too high. As discussed previously, this is likely due to a consistently warmer temperature in the model results. The bias appears to be fairly uniform and does not appear to produce significant differences between the observations and the model results. The geopotential height anomalies at 500hPa between the two phases of the AMO are quite similar in the observations (Figure 3.7a) and the model runs (Figure 3.7b). The model accurately reproduces the domain-wide negative geopotential height anomalies during the cold phase of the AMO. In both the observations and the simulations, the weakest anomalies occur in the southeastern U.S. and the strongest anomalies occur over the northern U.S. An anomalous trough occurs in both the observations and the model runs in the central U.S. and extends to the Gulf of Mexico. The magnitudes of the anomalies are similar between the observations and the model, with the greatest differences (of about 4m) occurring in the northern U.S. The reduced magnitude of the geopotential height anomalies in the central U.S. may be responsible for the reduced wind magnitude anomalies in the simulations in the southern U.S. Overall, the model simulations vary little from the observations in both the 10-year means and the anomalies for each phase of the AMO.

The model's ability to simulate the atmospheric circulations at 300hPa is somewhat weaker than at either 850hPa or 500hPa. Figures 3.8a and 3.8b show the observed and simulated wind and geopotential heights for JJA, respectively. The simulations produce geopotential heights in the central U.S. that are up to 40m lower than in the observations, suggesting a cold bias in the upper troposphere. The difference in the eastern U.S. is much smaller, with differences in the Ohio Valley of less than 10m. The

effect of this pattern is that the simulated ridge and trough system over the U.S. is much weaker than in the observations. The weaker ridge and trough produce nearly zonal flow in the simulations, whereas in the observations, there is a clear northerly component to the wind over much of the central and eastern U.S. as the flow enters the trough.

As with the simulations at 500hPa, the model is more capable of producing more accurate geopotential height anomalies at 300hPa than in simulating the mean conditions over the ten study summers. In the observations (Figure 3.9a), the entire eastern and central U.S. have negative geopotential height anomalies during the cold phase of the AMO, with the most negative anomalies occurring near Wyoming and the least negative anomalies occurring near Florida. This pattern produces southwesterly wind anomalies throughout much of the central and eastern U.S. in the cold phase. A similar pattern is found in the Reanalysis-forced simulations as well (Figure 3.9b). The overall magnitude of the negative anomalies is less than the observed anomalies, but the overall pattern is similar. The center of the strongest negative anomalies is also found in Wyoming, although it is offset to the southwest. The second anomaly center in the southeast is weakly positive in the simulations and is located west of its observed location. Like the observations, the model simulations produce a southwesterly wind anomaly throughout much of the central and eastern U.S.

Overall, the model is able to reasonably simulate the atmospheric circulations throughout the various levels of the troposphere. The model appears to be able to more accurately reproduce the anomalies between the phases of the AMO, than the average conditions over the entire simulation period. In the lower and middle troposphere, the

model has a warm bias, producing geopotential heights that are greater than in the observations. In the upper troposphere, there is a cold bias that produces simulated heights lower than observed. Despite the differences between the observations and the simulations induced by the temperature biases, the similarity in anomalies between the two datasets suggest that the model is accurately reproducing the relevant mechanism(s) that differs between the two phases of the AMO. As there are many forcings active within the Reanalysis data, it is impossible to state whether the forcing for this mechanism is the AMO; only that it changes between the years chosen for each phase of the AMO. In order to determine an AMO-forced mechanism, the AMO-forced simulations need to be analyzed.

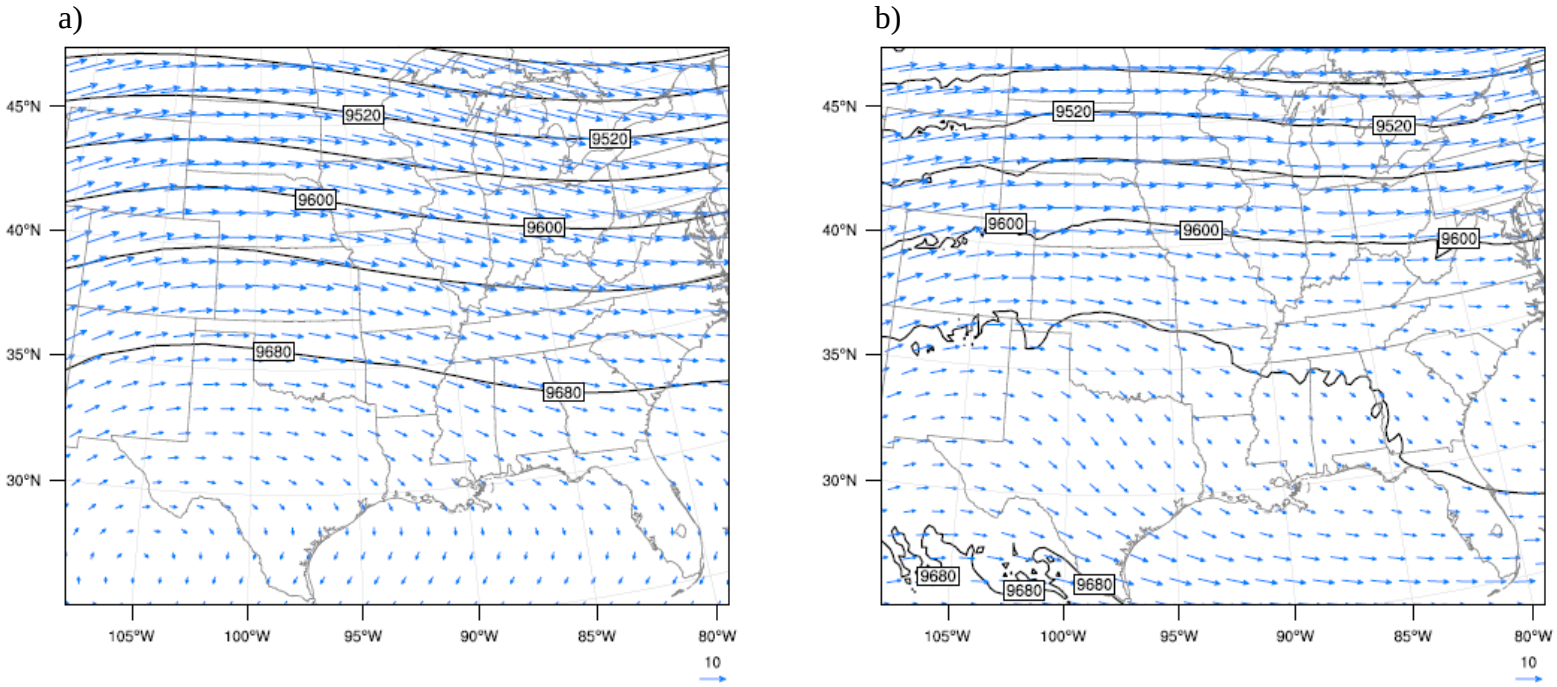

Figure 3.8 Mean (10-year) JJA 300hPa winds and geopotential heights for (a) the observations and (b) the Reanalysis-forced simulations. Units are in ms^{-1} (winds) and m (geopotential height). Reference vector is $10ms^{-1}$ and the contour interval is 40m with labels every 80m.

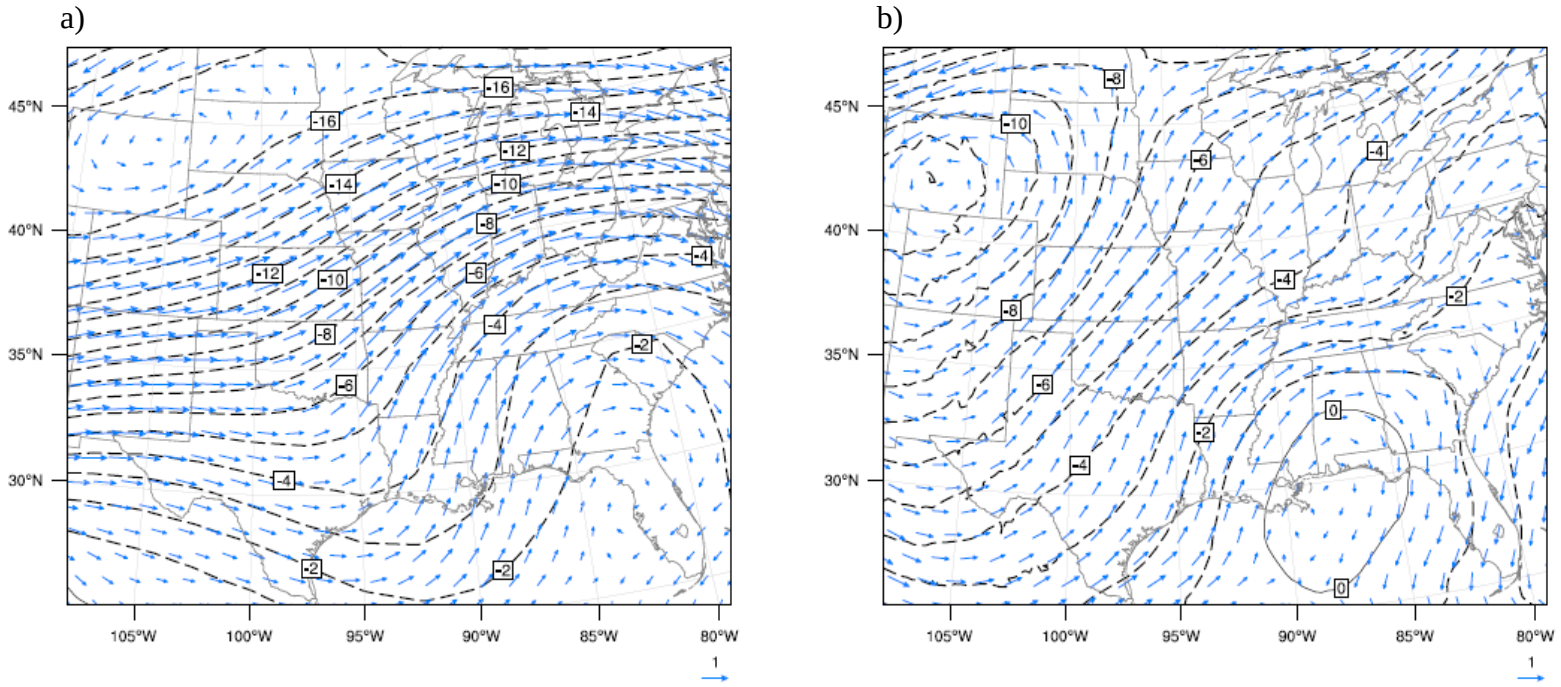

Figure 3.9 (a) Observed and (b) simulated JJA 300hPa wind and geopotential height anomalies for the cold phase of the AMO using the five selected years for the cold phase (1965, 1966, 1979, 1981, 1986). Units are in ms^{-1} (winds) and m (geopotential height). Reference vector is $1ms^{-1}$ and the contour interval is 1m with labels every 2m. Solid (dashed) lines indicate positive (negative) contours.

Chapter 4

Model Experiments and Results

4.1 Model Experiments

The previous chapter showed that WRF is capable of reasonably simulating the observed atmospheric circulations at the different levels of the troposphere as well as precipitation when forced by the Reanalysis data. Prior to the determination of any processes or mechanisms by which the AMO is able to influence the precipitation in the central U.S. from the AMO-forced model simulations, a general evaluation of the precipitation and atmospheric circulations is required to determine the performance of WRF when forced by the AMO.

The AMO-forced simulations are performed by driving the WRF model using the GCM output produced by AMO forcing only in Hu et al. (2011). The 10-year mean precipitation and the cold phase precipitation anomalies from the AMO-forced WRF simulations for JJA are shown in Figures 4.1 and 4.2a, respectively. The AMO-forced simulations produce much smaller magnitudes of precipitation across nearly the entire U.S. when compared to the Reanalysis-forced simulations (Figure 3.1b). The results indicate that during JJA, some areas receive only half of the precipitation as indicated by the Reanalysis-forced simulations and the observations. The difference in precipitation magnitude is most significant in the central and southern U.S., while the difference is smaller in the northern U.S. The difference is even greater near the Gulf of Mexico, where the AMO-forced simulations do not come close in capturing the precipitation

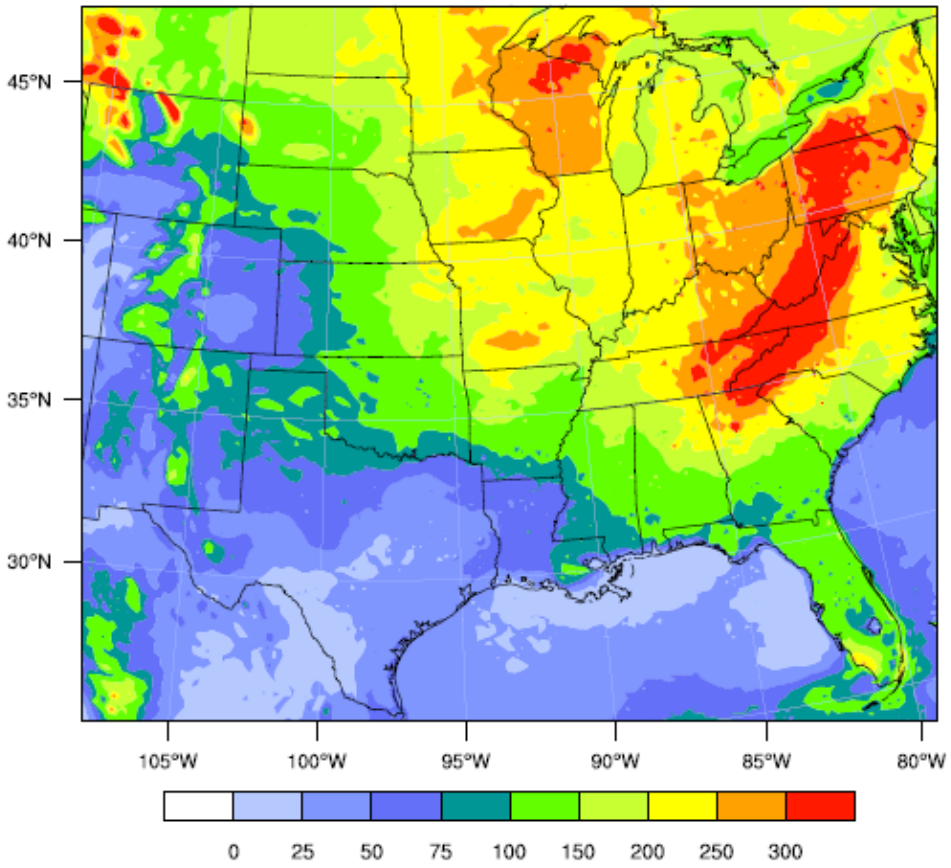

Figure 4.1 JJA mean (10-year) accumulated precipitation for the AMO-forced WRF simulations. Same scale used as in Figure 3.3. Units are in mm.

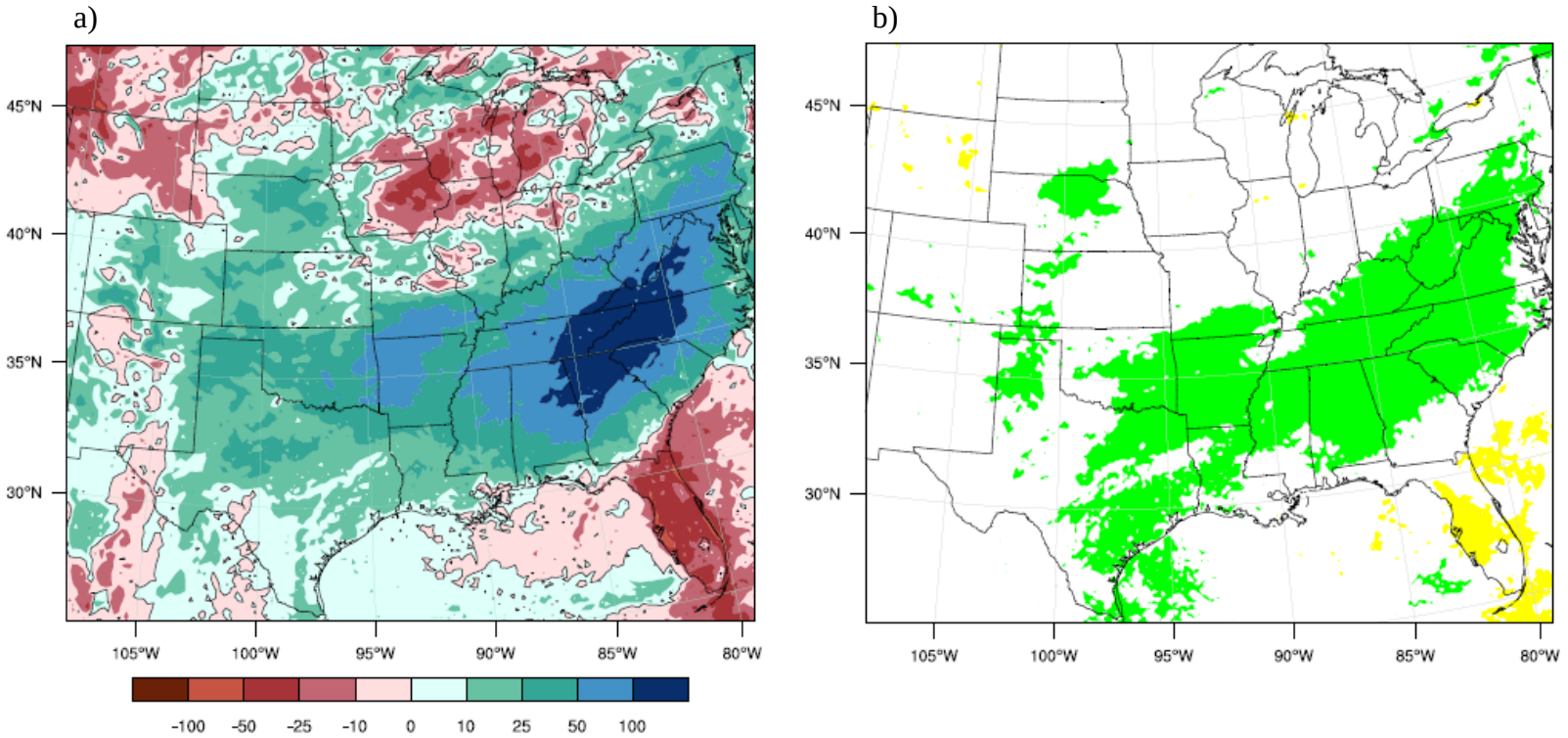

Figure 4.2 JJA cold phase (a) accumulated precipitation anomalies and (b) 95% significance of (a) for the AMO-forced WRF simulations. Same scale used in (a) as in Figure 3.4. For (b), green (yellow) indicates regions where positive (negative) anomalies are significant at the 95% confidence level. Units for (a) are in mm.

magnitude. As WRF is capable of reproducing reasonable precipitation quantities, as seen in the Reanalysis-forced simulations, these differences indicate that non-AMO forcings are important in producing the observed precipitation amounts.

Even though the magnitudes of the mean JJA accumulated precipitation in the AMO-forced simulations are substantially less than in the Reanalysis-forced simulations, the anomalies in each phase of the AMO are quite similar when the model is forced with the different forcings. The AMO-forced WRF simulations indicate above average precipitation in much of the central U.S., with the positive anomalies in central Nebraska and the south-central U.S. significant at the 95% confidence level (Figure 4.2b). The strong anomalies in the Appalachian Mountains are also significant, though as discussed previously, model bias may be the source of these anomalies. Below average precipitation in parts of the Midwest, north-central U.S. and Florida occur during the cold phase of the AMO. Central Florida contains the only negative anomalies during the cold phase that are significant at the 95% confidence level. This agrees well with previous studies that indicate that Florida has a significant increase in precipitation during the warm phase of the AMO (e.g. Enfield et al. 2001). The central U.S. does not contain any significant regions of decreased precipitation during the cold phase of the AMO.

The similarities in the AMO cold and warm phase anomalies between the Reanalysis and AMO-forced simulations are interesting because it occurs despite the Reanalysis-forced simulations being constrained by observations, as opposed to the idealized AMO only forcing present in the AMO-forced simulations. This suggests that the model is accurately capturing the processes forced by variations in the AMO and that

the AMO signal in the observations is strong enough to become apparent despite the presence of other forcings. Furthermore, the dissimilarities in precipitation magnitudes between the Reanalysis and AMO-forced WRF simulations suggest that there are processes unrelated to the AMO that affect the entire region but are unable to be reproduced by the model with AMO forcing only.

Next, we examine the lower atmospheric pressure fields. Compared to the Reanalysis-forced simulations, the AMO-forced WRF simulations produce somewhat greater geopotential heights across the U.S. (Figure 4.3). The AMO-forced simulations display a stronger mean summertime subtropical high pressure over the southeastern U.S. than is found in the Reanalysis-forced simulations. Initially, it appears as if WRF is significantly intensifying the subtropical high pressure. This is not what is occurring. The input data for the AMO-forced GCM simulations from Hu et al. (2011) contain a similar increase in 850hPa geopotential heights (their Figure 6a) from the observations used in this study. Beyond an increase in overall heights, the AMO-forced WRF simulations produce the same primary characteristics that are found in the observations and the Reanalysis-forced runs. The southeastern U.S. resides under the greatest geopotential heights from the western flank of NASH. The geopotential heights then decrease to the north and more rapidly to the west, with the lowest heights east of the Rocky Mountains in the northern U.S. near North and South Dakota.

In contrast to the AMO-forced 850hPa geopotential heights that share a similar pattern with the observations and only differ in magnitude, the mean JJA 500hPa geopotential heights display a different pattern, but similar magnitudes (Figure 4.4). The

AMO-forced simulations describe the high pressure in southern Texas and northern Mexico, but only a weak ridge in the central U.S. The geopotential height contours are more zonal than in the observations and the large scale ridge is found toward the east of its observed position. The eastward shift in location of the mean summer ridge could potentially be part of the cause for the significantly lower precipitation amounts in the AMO-forced model runs. In contrast to the means, the AMO-forced precipitation anomalies are fairly consistent with the observations, indicating that the mean geopotential heights at 500hPa may not be an important forcing for the precipitation anomalies. Rather, the location and magnitude of the geopotential height anomalies are important for the changes in precipitation, which the model was able to describe.

If compared to the Reanalysis-forced WRF simulations, the AMO-forced simulations have mixed results in simulating the observed mean precipitation, as well as the 850hPa and 500hPa heights. The model's ability to simulate the observed changes in precipitation between each phase of the AMO was much better, producing similar results to the Reanalysis-forced runs. This indicates that the model is able to accurately simulate the changes in the important parameters and dynamics that influence precipitation between the phases of the AMO.

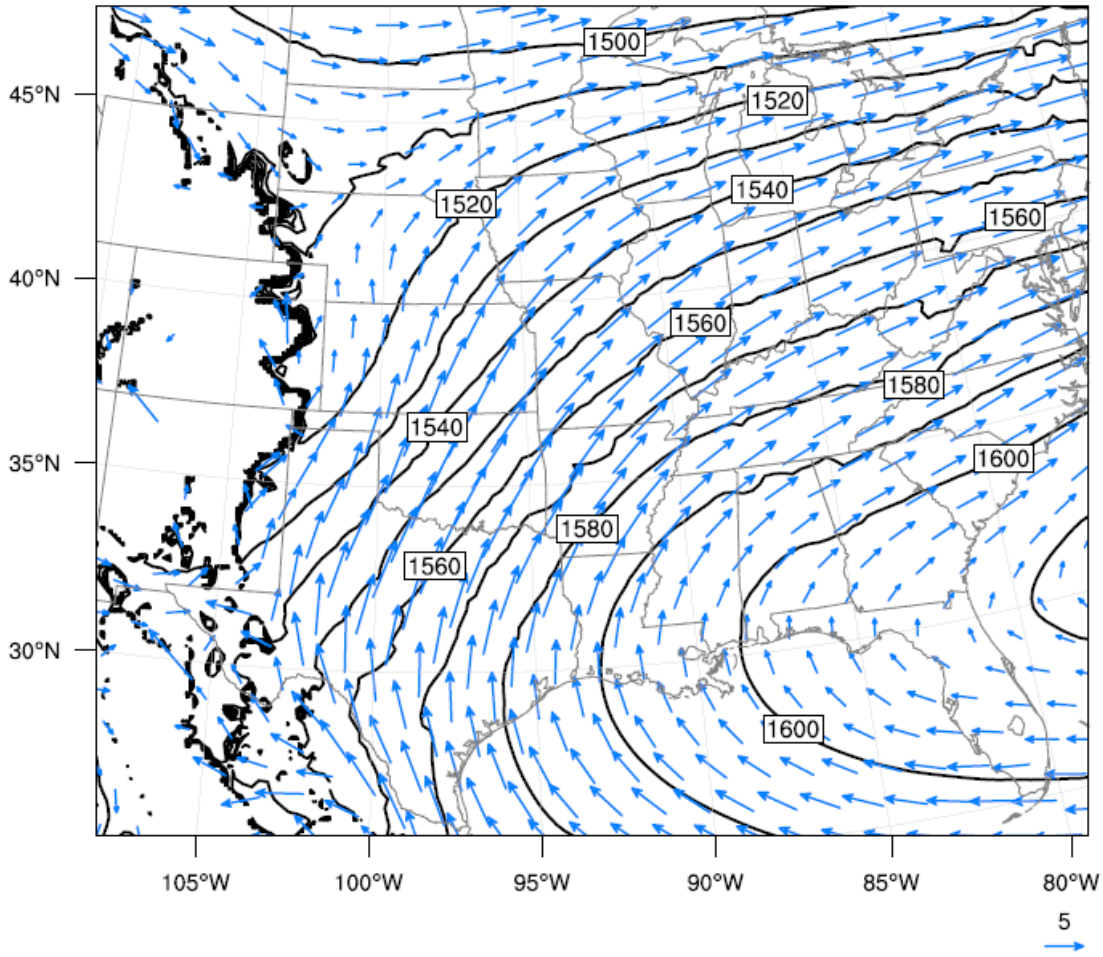

Figure 4.3 Mean (10-year) JJA 850hPa winds and geopotential heights for AMO-forced WRF simulations. Units are in ms^{-1} (winds) and m (geopotential height). Reference vector is $5ms^{-1}$ and the contour interval is 10m with labels every 20m.

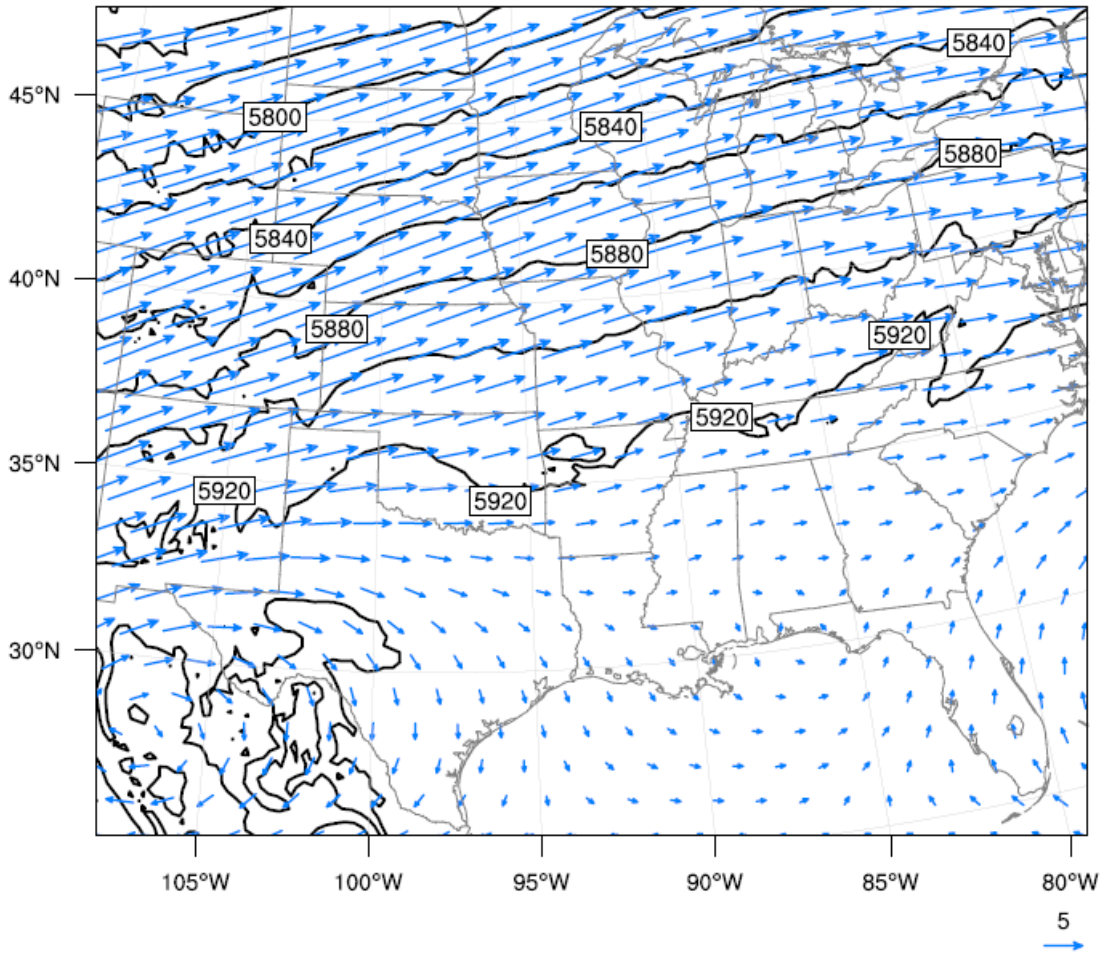

Figure 4.4 Mean (10-year) JJA 500hPa winds and geopotential heights for AMO-forced WRF simulations. Units are in ms^{-1} (winds) and m (geopotential height). Reference vector is $5ms^{-1}$ and the contour interval is 20m with labels every 40m.

4.2 Model Results

4.2.1 Lower Tropospheric Support

At decadal to multidecadal timescales, the amount of moisture in the atmosphere is approximately constant, producing a balance between the sources, sinks and transports of atmospheric moisture. For the atmosphere, there is only one significant process for each term; evaporation (source), precipitation (sink) and moisture divergence (transport). Any change in precipitation must be balanced by a corresponding change in either evaporation or moisture divergence. More specifically, any increase in precipitation must have an increase in evaporation or an increase in moisture convergence (decreased divergence). Without an increase in evaporation or a decrease in divergence, there would be a decrease in atmospheric moisture over time.

Evaporation is a local process, primarily dependent upon the available surface moisture and energy and to a lesser extent, local wind speed and temperature. Precipitation increases the moisture available at the surface, potentially increasing the evaporation rate. This recycling provides further support for precipitation without any additional external contributions to the local moisture budget.

Figure 4.5 shows the JJA average surface evaporation anomalies for the cold phase of the AMO. Most of the central and eastern U.S. experiences an increase in evaporation during the cold phase. The positive anomalies become more interspersed with negative anomalies in the north-central U.S. and are strongly negative in the central Midwest. In contrast to much of the land regions, the Gulf of Mexico displays negative (reduced) evaporation anomalies as a direct result of the decrease in the surface water

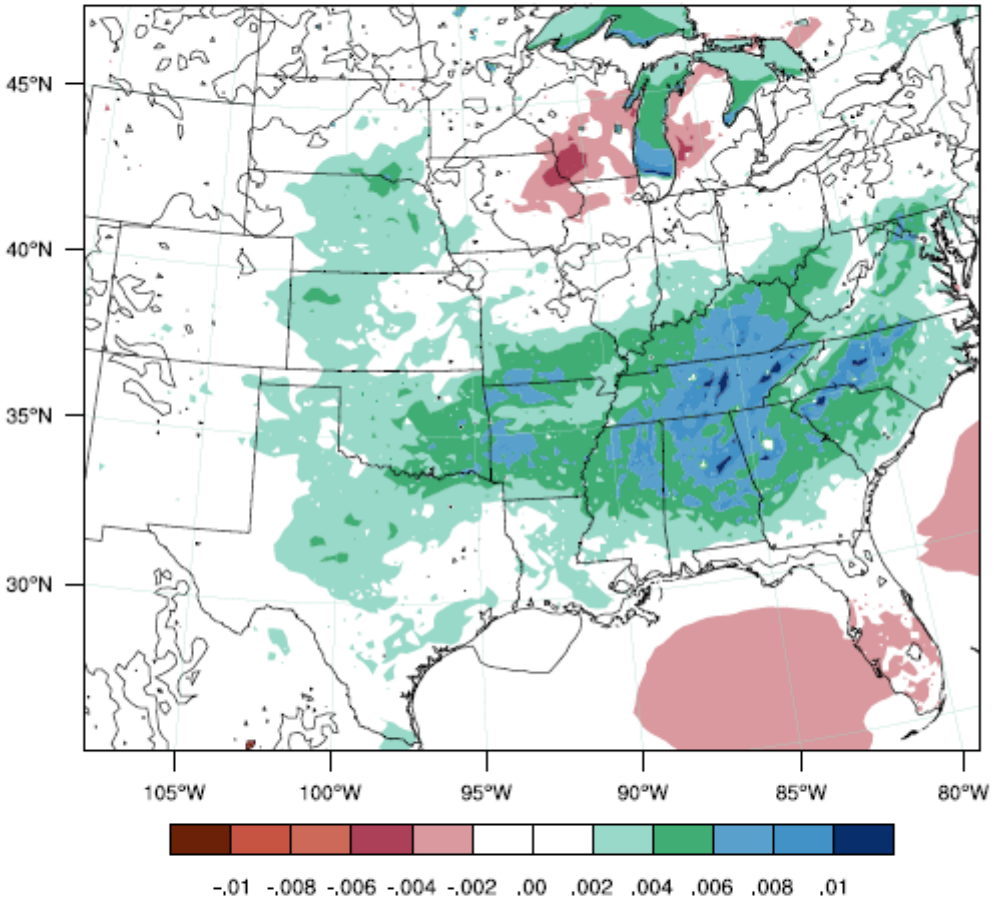

Figure 4.5 JJA cold phase anomalous upward moisture flux at the surface for the AMO-forced WRF simulations. Heavy line indicates the zero contour and magnitudes less than 0.002 are unshaded. Units are g m^{-2} s^{-1}.

temperature. Conversely, during the warm phase of AMO, much of the U.S. east of the Rocky Mountains experiences a decrease in evaporation with the exception of the central Midwest and parts of the north-central U.S., which has an increase in evaporation.

The increased evaporation during the AMO cold phase potentially provides some localized support for the increased precipitation that occurs. In the presence of external forcings (e.g., low-level moisture convergence and mid-level dynamic support), an increase of evaporation can support increased precipitation by providing additional moisture. At a minimum, the evaporation anomalies do not appear to hinder increased precipitation during the AMO cold phase. It has been shown that a reduction in soil moisture can further enhance drought conditions (Oglesby and Erickson, 1989). Applying this concept to the AMO, we see that by reducing soil moisture (and evaporation), the dry conditions of the AMO warm phase are further enhanced and the dry anomalies can become persistent. While evaporation has the potential to enhance the precipitation anomalies, other processes are likely more important, as the evaporation anomalies require a trigger. Variations in the low-level dynamic moisture flow can serve to initiate and sustain the precipitation anomalies.

To determine the low-level moisture flux and the variations with each phase in the AMO, we begin with the 850hPa geopotential heights to determine the circulation of the lower atmosphere. The geopotential heights at 850hPa are used as they provide an average pressure field for the lower troposphere and are approximately centered in the vertical for the low-level moisture flow (surface-700hPa). The most noticeable feature of the 850hPa geopotential height anomalies during the cold phase of the AMO (Figure 4.6)

is the presence of two anomaly centers, and part of a third pressure anomaly. The high pressure anomaly in the north-central U.S. dominates the central U.S. and Midwest, whereas the high pressure anomaly over the Gulf of Mexico and the subtropical North Atlantic controls the flow anomalies in the southern U.S. There is a low pressure zone between these two pressure systems that extends from Texas to New England. In New England, the low pressure anomaly becomes distinct enough to directly influence local circulations. The variations in geopotential heights between the cold and warm phases of the AMO are most prominent in the north-central U.S. and the Gulf of Mexico, where the heights can vary by as much as 20m. The variations between the cold and warm phases decrease toward the northeast, where there are a much smaller variations of 4-8m. The relatively small variations toward New England may explain why the anomalous circulations induced by the low pressure anomaly are relatively restricted to the northeastern U.S.

The positive geopotential height anomalies in much of the central and eastern U.S. indicate an intensification of the subtropical high pressure over the continental U.S. Recall from Figure 4.1 that the western flank and strongest gradients of NASH occur in the central U.S. The greater increase in pressure to the west of this boundary indicates that NASH is not only intensifying over its mean location, but expanding further toward the west during the cold phase of the AMO. Anomalies during the warm phase of the AMO indicate a different change in NASH. The strong reduction in pressure in the central U.S. indicates a recession of NASH from the central U.S. Furthermore, Hu et al. (2011) describe a northward shift of NASH during the AMO warm phase and this

appears to be supported by this study if the signs of the anomalies in Figure 4.6 are reversed to obtain the warm phase anomalies. During the warm phase, there is a slight low-level pressure increase in New England and this is likely due to the aforementioned northward transition of NASH.

The regional effect to the expansion and intensification of NASH during the cold phase of the AMO is to modify the pressure gradient at 850hPa throughout the central U.S. On an isobaric surface, the pressure gradient force is proportional to the gradient of the geopotential height. Anomalies of the pressure gradient force magnitudes for the cold phase of the AMO are shown in Figure 4.7. During the cold phase, much of the central U.S. experiences a weakening of the pressure gradient force. This is directly caused by the expansion and variable intensification of the subtropical high pressure system in the region. The pressure increases more rapidly in the north-central U.S. than it does toward the south or east. This results in reducing, rather than simply relocating, the strongest pressure gradients. This is because the strong gradient that exists between the high pressure in the southeast and the lower pressures in the central U.S. is approximately stationary in both phases of AMO (Figure 4.8). Due to the approximately stationary position of the strongest pressure gradients, any change of pressure gradient across that boundary reduces the pressure gradient force in the region rather than relocating the boundary to a new location. A similar process occurs during the warm phase of the AMO. Once again, the boundary of strong pressure gradients is approximately stationary. As the high pressure retreats from the west, the pressure over the north-central U.S. drops more rapidly than the areas to the east as it is released from the

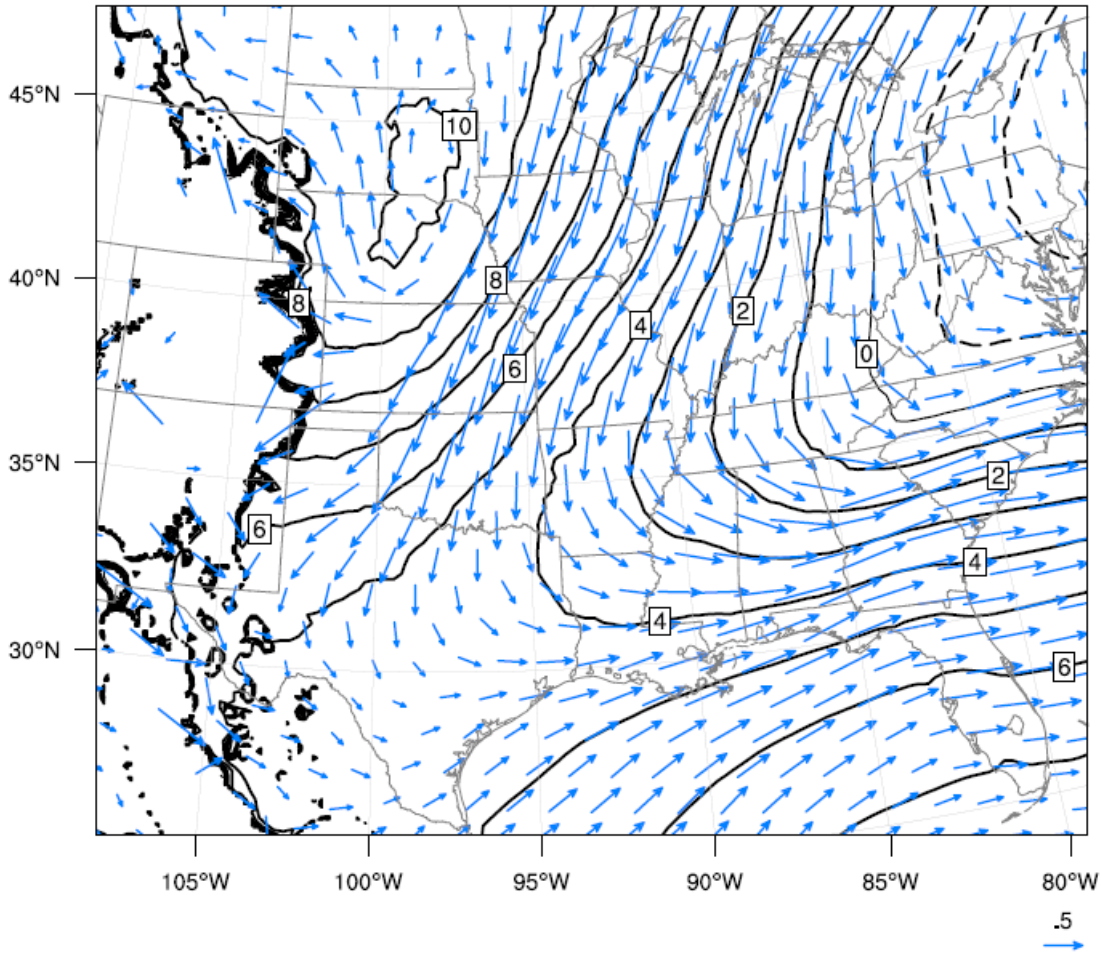

Figure 4.6 JJA 850hPa wind and geopotential height anomalies for the cold phase from the AMO-forced WRF simulations. Units are in ms^{-1} (winds) and m (geopotential height). Reference vector is $0.5ms^{-1}$ and the contour interval is 1m with labels every 2m. Solid (dashed) lines indicate positive (negative) contours.

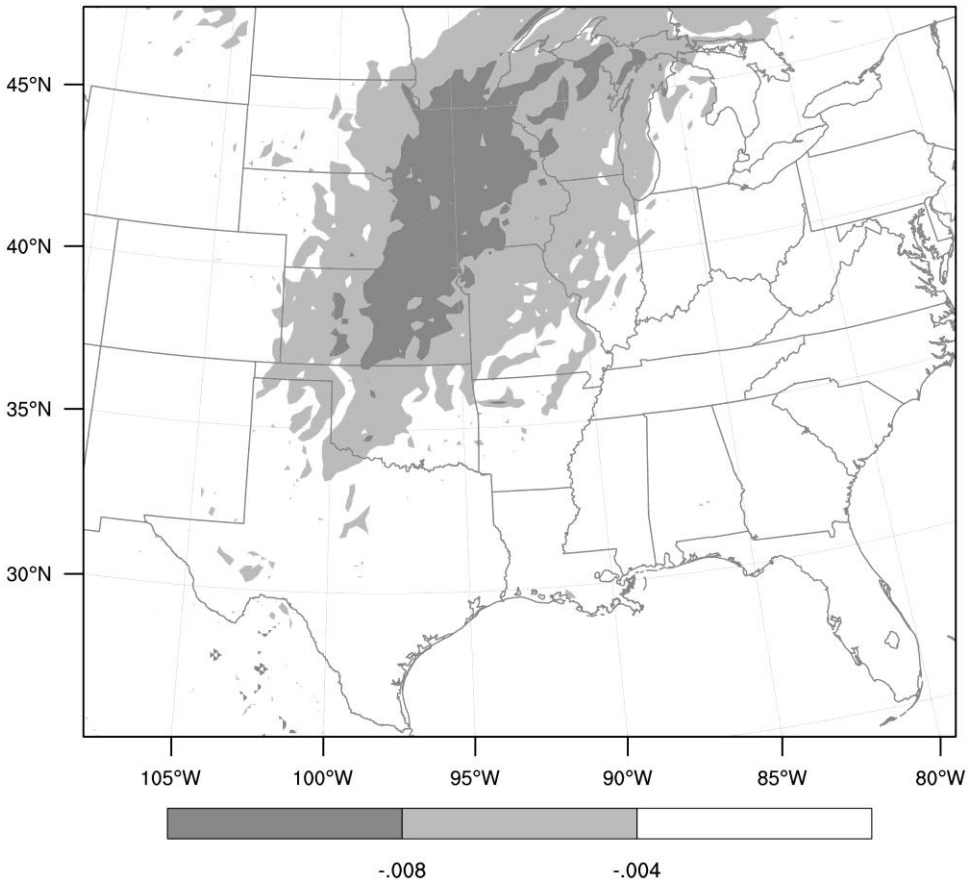

Figure 4.7 JJA pressure gradient force anomalies at 850hPa during the cold phase of the AMO. Values less than -0.004 are shaded.

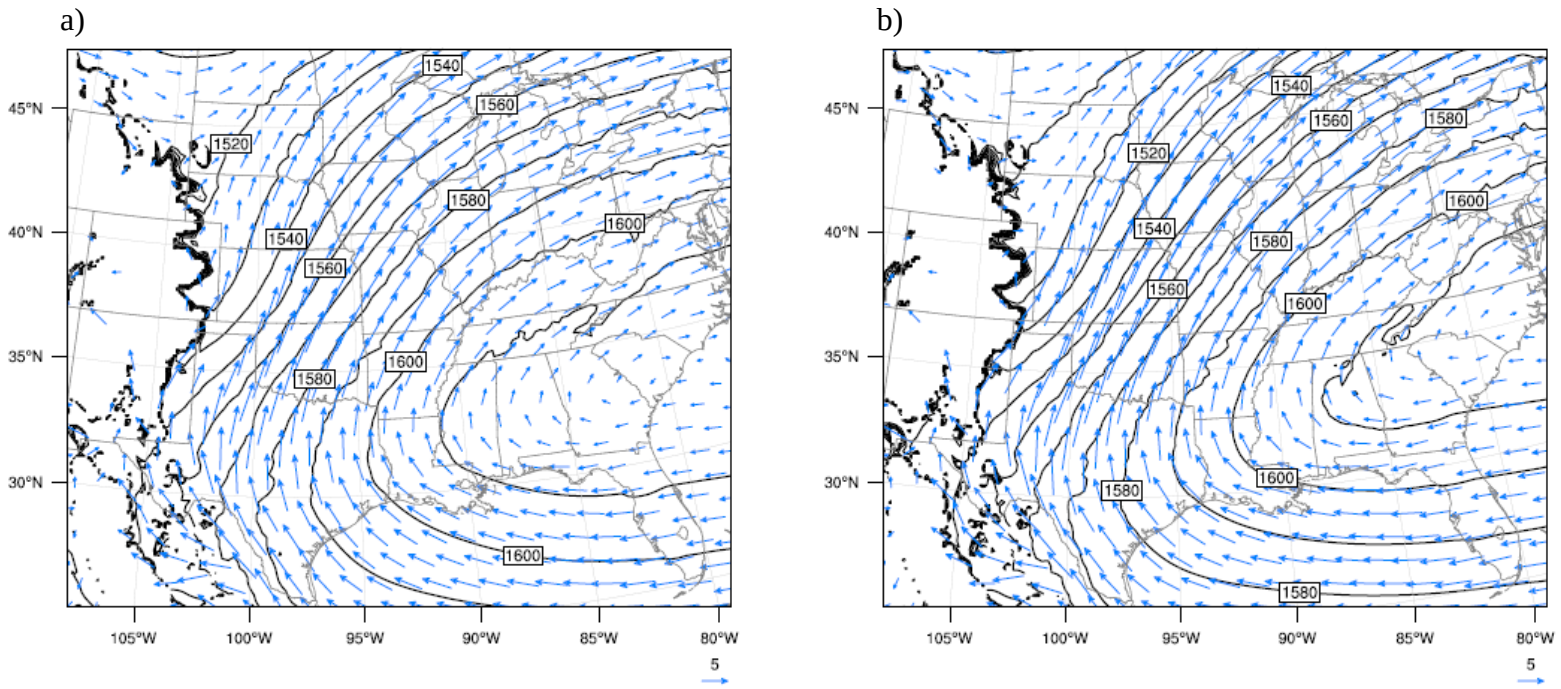

Figure 4.8 Mean JJA 850hPa geopotential heights for the (a) cold and (b) warm phases from the AMO-forced WRF simulations. Units are in ms^{-1} (winds) and m (geopotential height). Reference vector is $5ms^{-1}$ and the contour interval is 10m with labels every 20m

influence of the high pressure system. The more rapid drop in pressure in the west causes an increase in the pressure gradient and the resultant force.

The changes in the pressure gradient force are not homogenous in the central U.S. The north-central U.S. experiences greater changes between the phases of the AMO, than the regions to the south. In the north-central U.S., the expansion of the high pressure occurs to the north and the west, reducing the pressure gradient force in both the meridional and zonal directions. In the central U.S., the high pressure expands zonally, but intensifies uniformly in the meridional direction. It is the expansion of the high pressure that is the primary cause of the change in the pressure gradient forces rather than the intensification. The expansion in only one direction reduces the weakening in pressure gradient force when compared to the reductions that occur in the north-central U.S. The net result of these changes is that the greatest reductions in pressure gradient force occur in the north-central U.S. Likewise, during the warm phase of the AMO, the greatest increases in pressure gradient occur in the north-central U.S. as the high pressure retreats from both the north and the west, sharply increasing the pressure gradient in the area.

The key effect on the circulation due to the change in pressure gradient force between the phases of the AMO is to modify the low-level southerly flow into the central U.S. The weakened southerly flow during cold phase is a direct result of the weakening of the pressure gradient force. The intensification of the pressure gradient force during warm phase strengthens the southerly flow throughout the central U.S. As with the pressure gradient force anomalies, the wind anomalies vary throughout the central U.S.

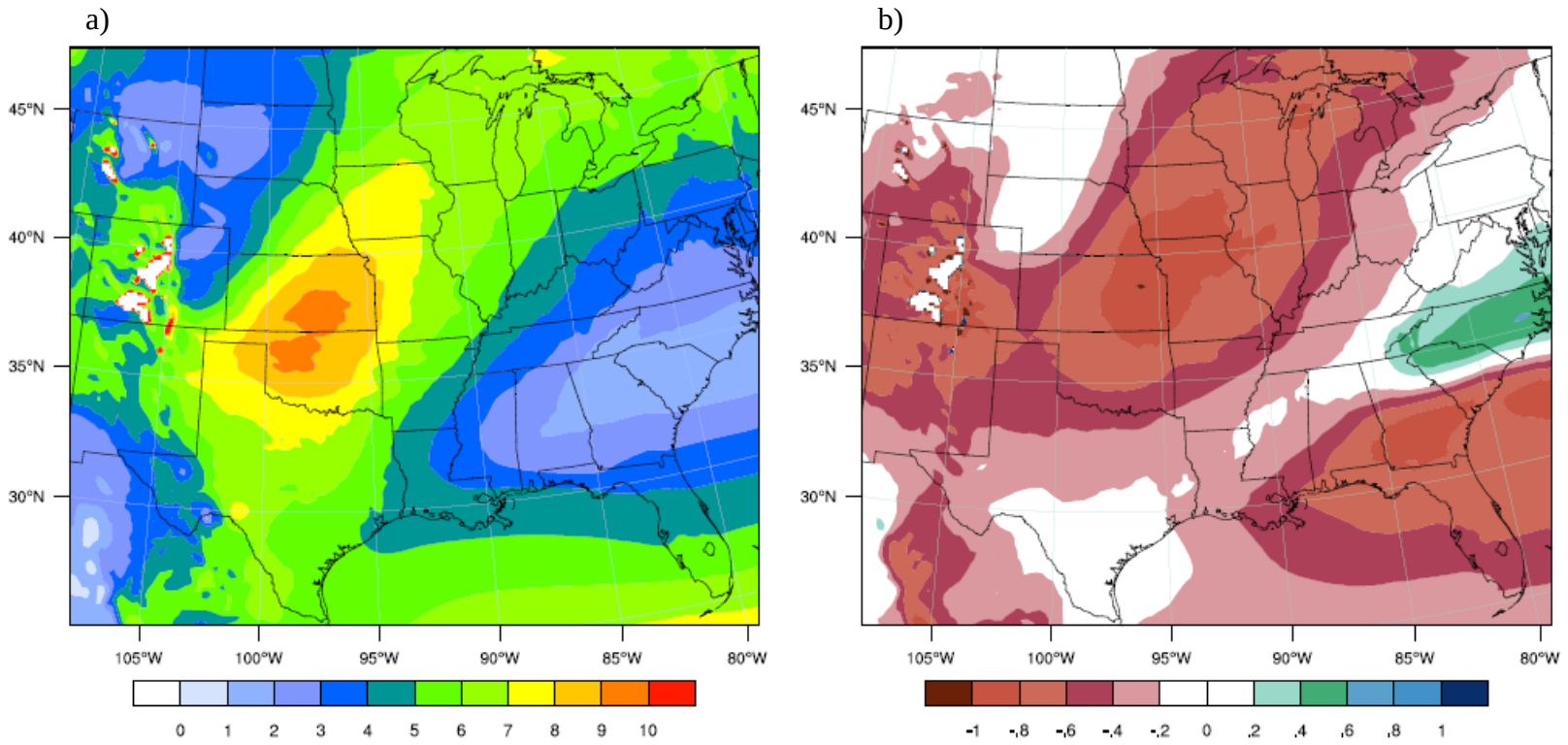

Figure 4.9 JJA surface-700hPa (a) mean (10-year) wind magnitudes and (b) cold phase anomalies for the AMO-forced simulations. Units are in ms^{-1}.

To determine how the change in pressure gradient force affects the wind, the magnitude of the average JJA wind for the lower atmosphere (surface-700hPa) is shown in Figure 4.9a. This average was calculated by vertically integrating the wind from the surface to 700hPa and then dividing by the difference between the average surface pressure and 700hPa. The maximum wind speed occurs in the central U.S., where the pressure gradient is strongest. The impact of the spatial variations in the pressure gradient force anomalies on the wind magnitudes can be seen in Figure 4.9b. The greater decrease in the pressure gradient force in the north-central U.S. during the cold phase weakens the wind speed more in the north than in the south. This results in a decreased wind maximum in the central U.S. and an even greater decrease in wind speed north of the maximum. The result of this is that the southerly wind, relative to the warm phase of the AMO, slows as it progresses north.

These changes in the low-level wind flow modify the low-level divergence and associated moisture fluxes. The surface-700hPa vertically integrated moisture flux (hereafter, "moisture flux") is a useful diagnostic in examining how the wind fields redistribute the low level moisture. As one would expect, anomalies in the low level moisture flux (Figure 4.10) are very similar to the 850hPa wind anomalies (Figure 4.6) during the cold phase of the AMO. Northerly moisture flux anomalies dominate the central U.S. during cold phase, indicating reduced transport of moisture out of the central U.S. Increased southerly transport of moisture occurs during warm phase, as indicated by the southerly anomalies. The decreased moisture flux out of the central U.S. during the cold phase indicates that there is a relative convergence of moisture. A convergence

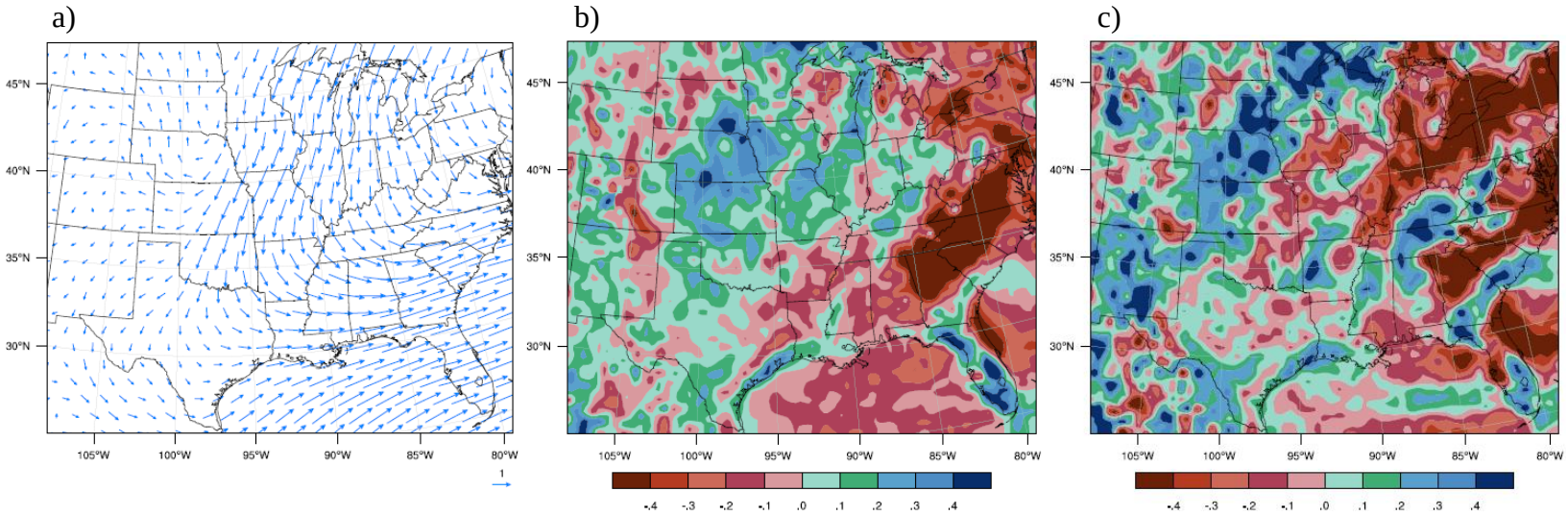

Figure 4.10 (a) JJA surface-700hPa vertically integrated moisture flux anomalies during the cold phase of the AMO. (b) JJA and (c) August divergence of the vertically integrated moisture flux during the cold phase. Units are (a) kg kg^{-1} Pa and (b,c) 10^{-5} g kg^{-1} s^{-1}. Unit vector is 1 kg kg^{-1} Pa.

anomaly is supportive for increased precipitation by providing an increase in the moisture available for precipitation

The effect of the gradual slowdown in wind speed to the north, relative to warm phase, is that there should be a region of convergent moisture anomalies in the central U.S., from Texas to the region of maximum negative anomalies. This is what the model simulates for two of the three months during summer, especially during August. During July, the model simulates widespread moisture divergence during the cold phase over most of the central U.S. There is still increased precipitation during the cold phase, indicating that the moisture divergence must be, and is, compensated for by an increase in evaporation. The result of these processes is that the JJA moisture flux indicates divergence over the central U.S. during cold phase. Figures 4.10b and 4.10c show the JJA and August moisture flux divergence anomalies for the cold phase of the AMO. During August, the moisture flux convergence anomalies from the wind convergence anomalies are clearly visible in the central U.S.

Though not a perfect match, the regions of increased precipitation during the cold phase in the central U.S. generally occur in the same areas that experience moisture convergence anomalies. The moisture anomalies provide the additional moisture required to sustain the increased precipitation that occurs during the cold phase of the AMO. As such, the spatial and temporal changes in the pressure gradient over the central U.S. form an integral part of the mechanism in which the AMO influences the summer precipitation over the central U.S.

4.2.2 Vertical Moisture Profiles

Precipitation is not only dependent on available moisture but also on atmospheric stability. In general, increasing the moisture content in a region will only produce an increase in precipitation if there is a trigger to initiate a process that converts the accumulated moisture into precipitation. In order to enhance precipitation during the cold phase of the AMO, there must be support for upward vertical motions in the regions that experience increased precipitation. One potential source of vertical motions is an increase in atmospheric instability. The vertical profile of the atmosphere can be examined to see whether there is increased instability during the AMO cold phase.

Figure 4.11 shows the geographical location of three different cross-sections used in this analysis. The first cross-section ("A" in Figure 4.11) spans from the northeastern corner of Texas to approximately Detroit, Michigan. The second and third cross-sections ("B" and "C" in Figure 4.11) originate at the same location in Texas, but terminate in central Wisconsin and central Minnesota, respectively. For simplicity, the cross-sections will be referred to as the eastern, central and western cross-sections (A-C in Figure 4.11, respectively). Figures 4.12 show the mean (10-year) JJA water vapor mixing ratios for all three different cross-sections. In all three cross-sections, the average near surface moisture content decreases toward the north as the flow moves farther from the main source of moisture in the Gulf of Mexico. In the western cross-section (Figure 4.12c), surface moisture decreases more rapidly than in the other two cross-sections, despite the closer geographical proximity to the terminal point of the central cross-section (Figure

4.12b) than the central cross-section is to the eastern cross-section (Figure 4.12a). The spatial variations in moisture essentially disappear in the low moisture mid-troposphere.

For the eastern cross-section, there are significant changes in JJA moisture content between the phases of the AMO. During cold phase, the increased moisture content from moisture convergence anomalies are visible below 750hPa (Figure 4.13a). The most striking feature in this profile is the drier air (negative anomalies) near 650hPa that overlies the near-surface moist air. The dryness in terms of the mixing ratio at 650hPa can be as much as 5% of the mean mixing ratio at that level. Whereas the increase in moisture below 650hPa is closer to about 3% of the mean, although the magnitude of the increase near the surface is still greater, due to the much higher mean moisture content of the lower troposphere. The placement of drier air over more moist air produces an atmospheric profile that is more convectively (potentially) unstable during the cold phase of the AMO. With this vertical profile of moisture anomalies, atmospheric disturbances would be more prone to generate convective precipitation, which is the primary form of precipitation during the summer months in the central U.S. During the warm phase of the AMO, the anomaly pattern is reversed. The moisture divergence anomalies and reduced evaporation leave the lower atmosphere with reduced moisture and is overlain by relatively moist air. This produces a more stable atmospheric profile that suppresses convective development during the warm phase.

During the cold phase of the AMO, the drier air aloft is an important component in producing a more unstable atmospheric profile. To determine the source of the dry air, we can examine the 700hPa wind anomalies (Figure 4.14). During the cold phase,

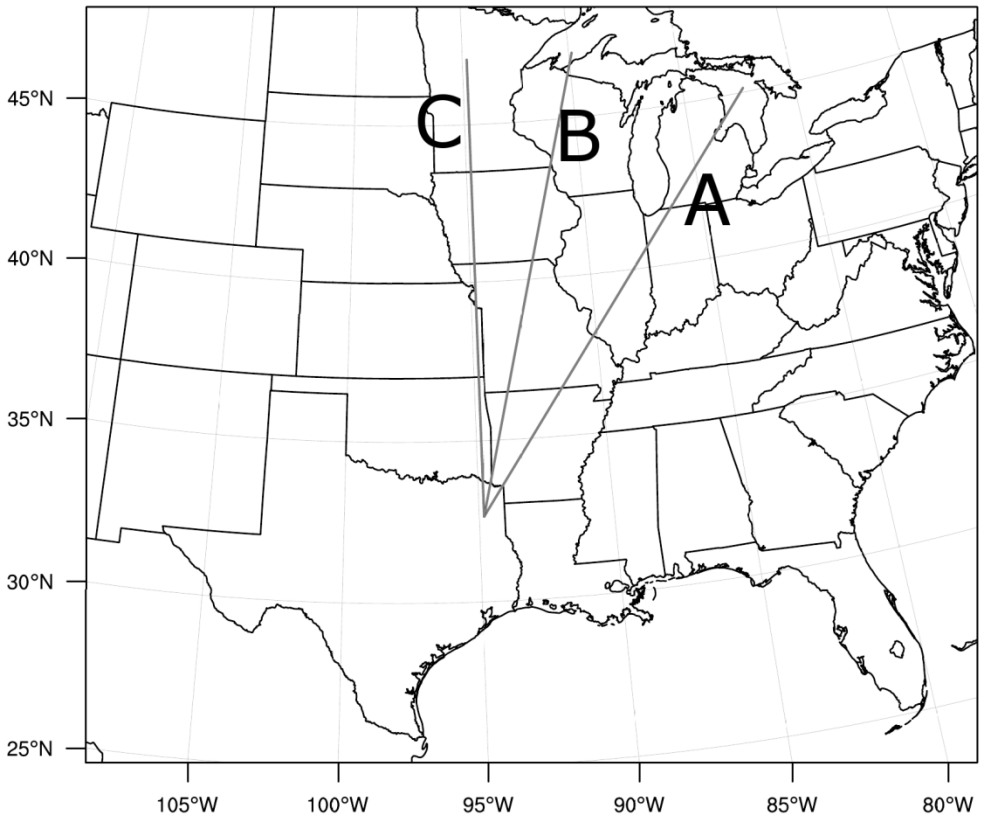

Figure 4.11 Map showing the locations of the eastern (A), central (B) and western (C) cross-sections described in the text.

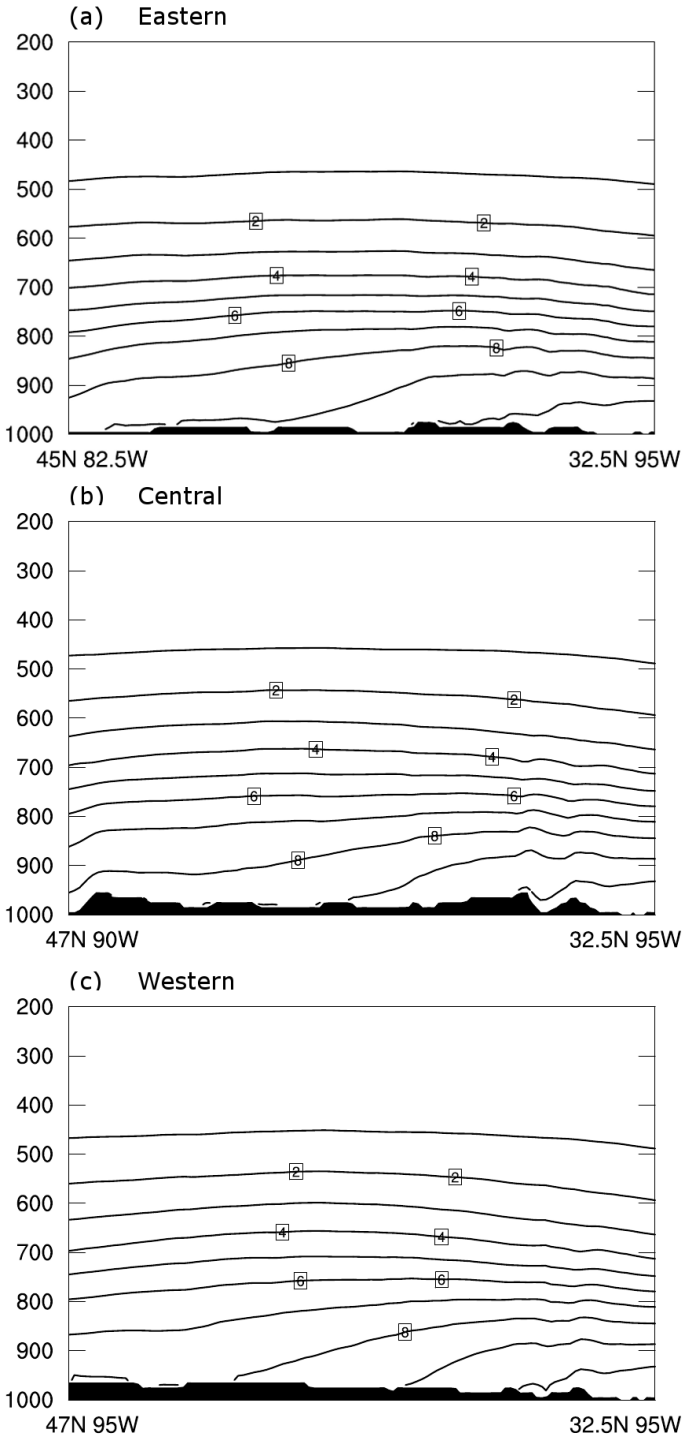

Figure 4.12 Mean JJA moisture cross-sections during the cold phase for the (a) eastern, (b) central and (c) western cross-sections. Vertical axis is pressure and horizontal axis is the location. Units are in g kg^{-1} and contour interval is 1 g kg^{-1} with labels every 2 g kg^{-1}.

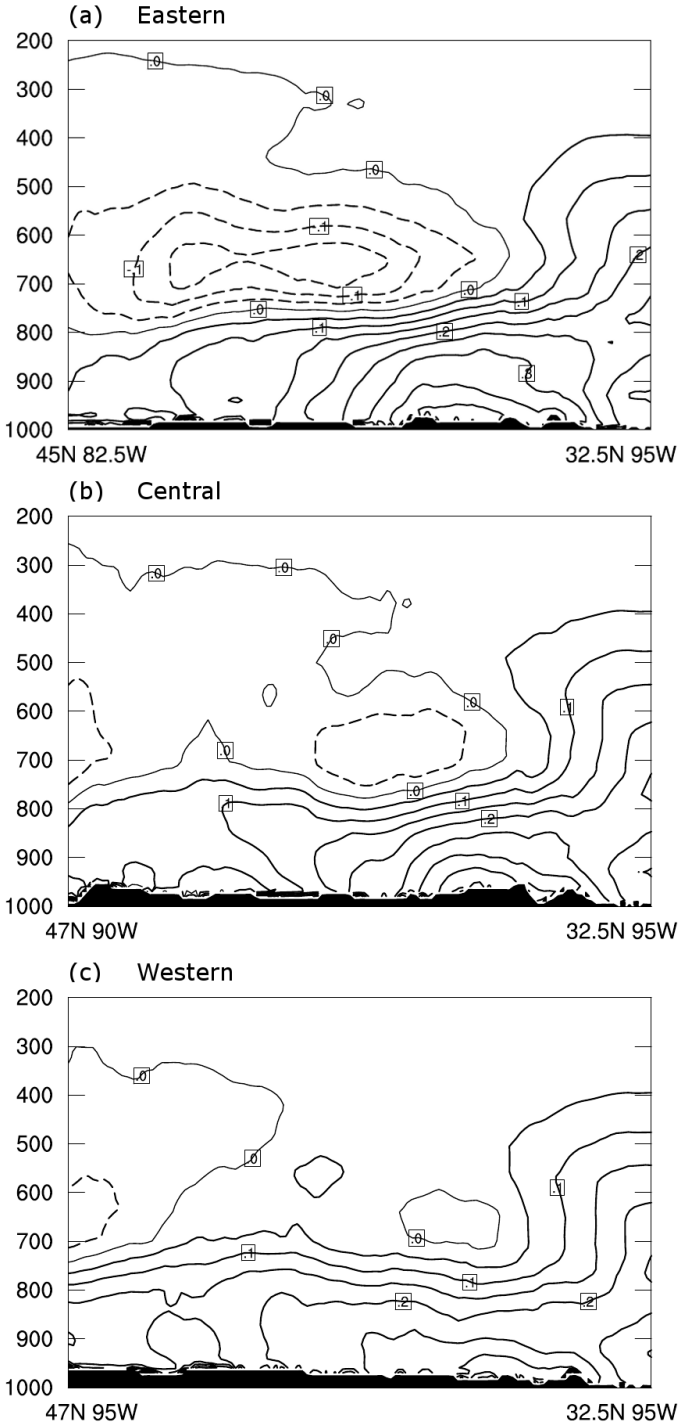

Figure 4.13 JJA cold phase moisture anomalies for the (a) eastern, (b) central and (c) western cross-sections. Vertical axis is pressure and horizontal axis is the location. Units are in g kg^{-1}. Contour interval is 0.05 g kg^{-1} with labels every 0.1 g kg^{-1}. Solid (dashed) lines indicate positive (negative) contours.

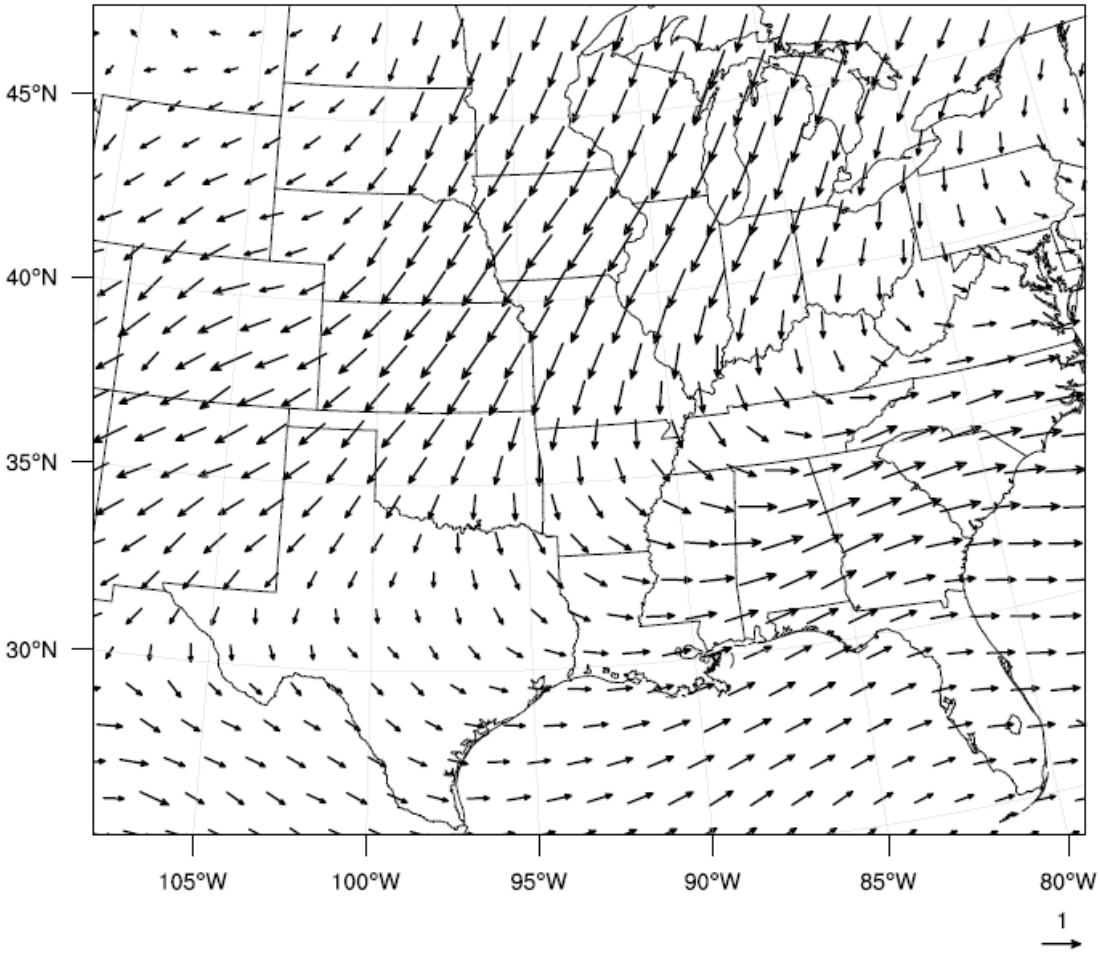

Figure 4.14 JJA 700hPa wind anomalies for the cold phase of the AMO from the AMO-forced WRF simulations. Units are in ms^{-1}. Reference vector is $1ms^{-1}$.

northerly flow anomalies prevail over much of the central U.S. Northerly anomalies indicate that there is a reduction in the moist flow from the Gulf of Mexico into the central U.S. and Midwest. The reduction in the wind's meridional magnitude is greater than the zonal reduction; indicating a decrease in wind speed and a shift from southerly to southwesterly winds. This places the origin of the 700hPa flow near the dry air of the desert southwest and northern Mexico. This anomalous flow contributes to the drier air that near 650hPa that overlies the low-level moist air (Figure 4.13).

During the warm phase, the wind anomalies are southerly, indicating an enhanced flow out of the moist southerly air mass over the Gulf of Mexico. The moist air enters the central U.S. and contributes to the moistening of the near surface air, thus stabilizing the atmosphere by reducing the potential instability of the atmosphere.

The change in the 700hPa flow between the two phases of the AMO is most likely attributable to the expansion of NASH during the cold phase. As shown in Wang et al. (2007), expansion of NASH due to cold North Atlantic SSTs is most pronounced in the latitudes near 25-30°N, nearly reaching the North Pacific Ocean. The ridge then makes a sharp turn to the northeast and traverses from the desert southwest to the central U.S. Similarly to this current study, Wang et al. (2007) found that with a warm North Atlantic, NASH recedes eastward. The western flank is nearly meridional and is located much closer to the central U.S. The change in the flow at 700hPa between the two phases of the AMO agrees with these findings. The dominant flow out of the southwest during cold phase occurs on the western flank of the expanded NASH. During warm phase, the

western flank is closer to the central U.S., allowing for a direct flow of moist Gulf air to mix with the southwesterly flow.

The more convectively unstable atmospheric profile found during cold phase in the eastern cross-section coincides with positive precipitation anomalies. If this process is an important part of the mechanism driving the precipitation anomalies, it should be weaker in the north-central U.S., where precipitation anomalies are weakly positive during the cold phase. Figures 4.13b and 4.13c show the moisture anomalies for the central and western cross-sections, respectively. The central cross-section displays a similar anomaly pattern as the eastern cross-section, though with reduced magnitudes. The increased moisture near the surface during the cold phase is mostly limited to the southern two-thirds of the cross-section, with only weak anomalies further to the north. Likewise, negative moisture anomalies at 650hPa are found in the southern part of the cross-section. Similar to the moist anomalies at the surface, the magnitudes are weaker and nearly vanish in the northern part of the cross-section, except in the extreme north, where the negative anomalies intensify. The weakening of the unstable profile in the north coincides with reduced precipitation during the cold phase of the AMO (Figure 4.2). In the far northern Midwest, the anomalously unstable profile is partially reestablished and corresponds to a small area of positive precipitation anomalies.

For the western cross-section, the moisture anomaly pattern in the south is similar to the other two cross-sections. As with the central cross-section, the moisture accumulation in the lower levels during cold phase is not as pronounced as it is along the eastern cross-section. It is in the mid-levels that a noticeable departure from the other

two cross-sections occurs. The negative moisture anomalies found in the other two cross-sections do not exist in the western cross-section, replaced by weak positive anomalies. The exception to this is over Minnesota, where a weak pattern of moist air near the surface is overlain by drier air above it. Negative precipitation anomalies occur over much of the area in which the convectively unstable anomalies are absent. In Minnesota, the precipitation anomalies become mixed, with some positive anomalies during cold phase. This is also the region in which a weaker form of the unstable anomalies is present.

The weaker and less pronounced moisture anomalies at 650hPa for the central and western cross-sections are still consistent with the stronger anomalies in the east. During the warm phase of the AMO, the moist southerly flow at 700hPa is able to penetrate much further to the north than in cold phase. With a weaker connection to the moist air from the Gulf of Mexico during both phases of the AMO, the northern U.S. experiences little variation in mid-level moisture content between the phases of the AMO.

The precipitation anomalies and the moisture profiles for the three cross-sections imply that there is a strong connection between increased precipitation during cold phase and the convectively unstable anomalies. All three cross-sections contain positive moisture anomalies near the surface overlain by negative anomalies in the areas with increased precipitation. In the western and central cross-sections, the cold phase connection to the dry air at 700hPa is weaker toward the north, producing a less unstable atmospheric profile and decreased precipitation during the cold phase. Whereas in the south, the strong increase in low-level moisture and weak drying in the overlying layer

contribute to a weak increase in convective instability and increased precipitation. As strong as the connection appears to be between the convectively unstable anomalies during the cold phase of AMO and increased precipitation, the moisture profile only supports increased precipitation and cannot be the sole cause of it, as vertical lift is still required. The more unstable profile present during cold phase provides support for any passing disturbances, allowing for a greater potential to produce precipitation.

4.2.3 Middle Tropospheric Support

The accumulation of moisture near the surface and the anomalously unstable atmospheric profile serve to provide support for precipitation anomalies, but they are not the sole source of the anomalies. Similarly, the increased moisture in the lower atmosphere and the more convectively unstable atmospheric profile during cold phase provide support for precipitation, but do not create the disturbances required to utilize this supportive environment and release the instability. This instability can be utilized if it occurs along with a supportive dynamic background environment. The middle troposphere can be a source for this dynamic support. As such, we will next examine the atmospheric circulations of the middle troposphere.

The 500hPa geopotential heights describe the mass distribution of the middle troposphere and serves as an initial point in the analysis of the middle troposphere. Figure 4.15 shows the mean 500hPa geopotential heights for the cold (Figure 4.15a) and warm (Figure 4.15b) phases of the AMO. During cold phase, the geopotential height contours are nearly zonal, with a small ridge in the central U.S. that is superimposed over

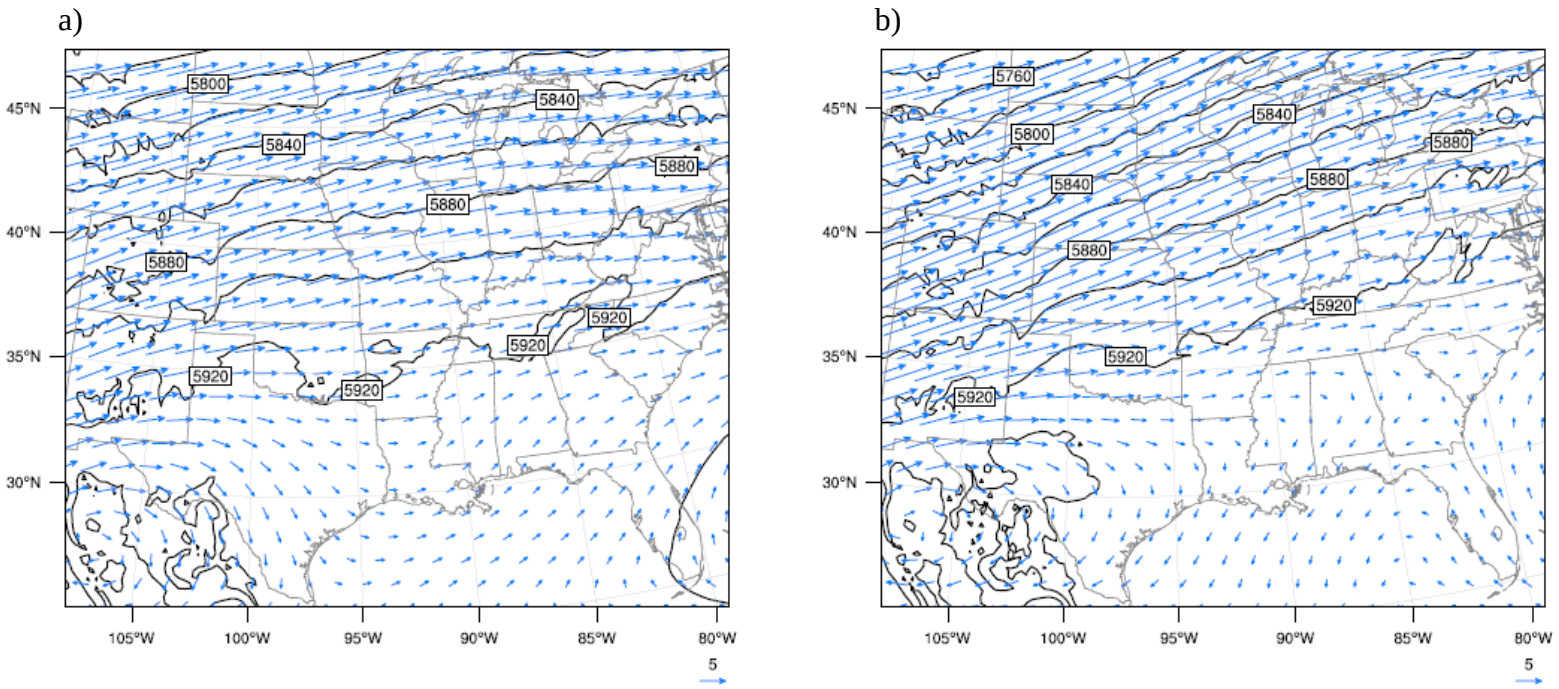

Figure 4.15 Mean JJA 500hPa geopotential heights for the (a) cold and (b) warm phases from the AMO-forced WRF simulations. Units are in ms^{-1} (winds) and m (geopotential height). Reference vector is $5ms^{-1}$ and the contour interval is 20m with labels every 40m.

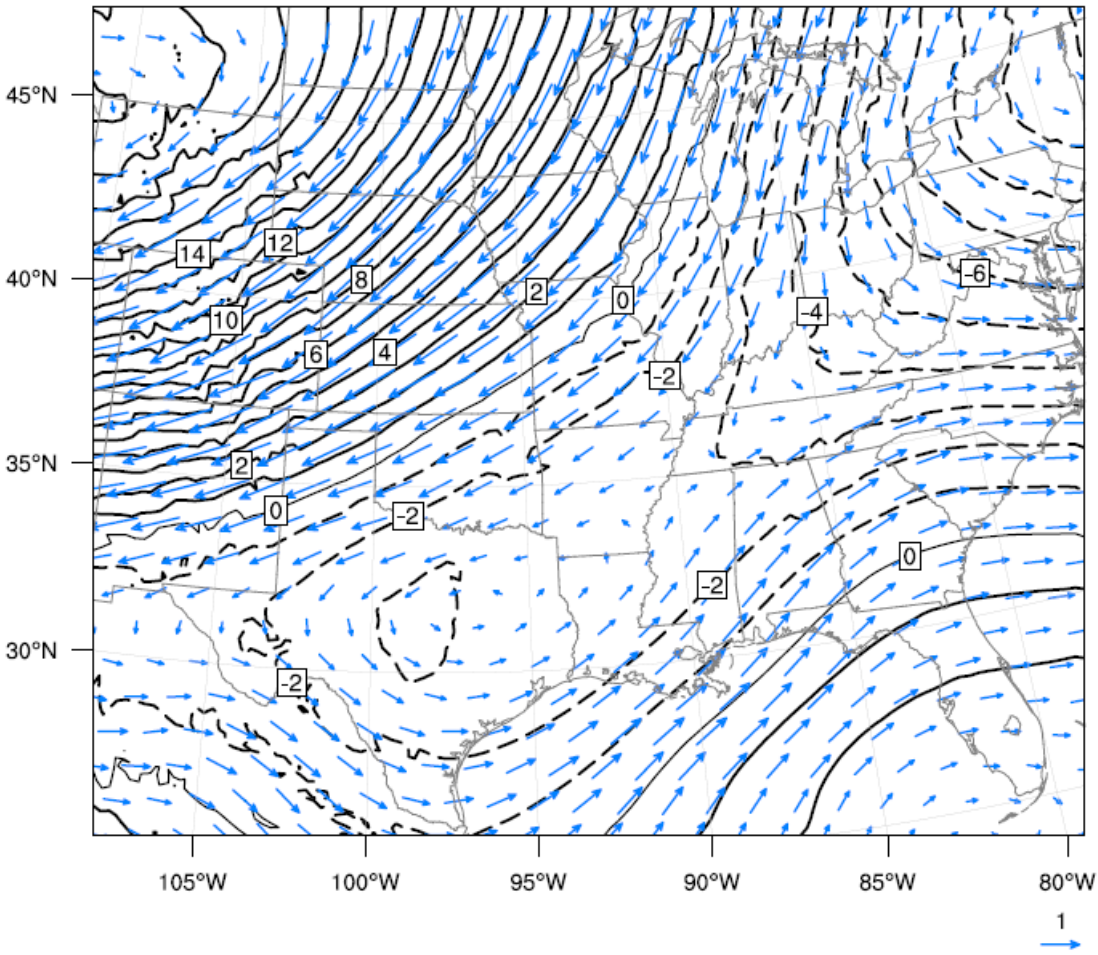

Figure 4.16 JJA cold phase 500hPa geopotential height and wind anomalies. Units are in ms^{-1} (winds) and m (geopotential height). Reference vector is $1ms^{-1}$ and the contour interval is 1m with labels every 2m. Solid (dashed) lines indicate positive (negative) contours.

a larger scale pressure system slight tilt toward the northeast. The central U.S. ridge is more prominent in the south-central U.S. During the warm phase of the AMO, the tilt of the large-scale system toward the northeast becomes much more pronounced. These features are interesting in that the model lessens the magnitude of the observed ridge over the central U.S. and shifts it toward the east. Further analysis of the anomalies provides additional details on how the structure changes between the phases of AMO.

Similarly to the 850hPa geopotential height anomalies during the cold phase of the AMO, the 500hPa geopotential heights display three distinct anomalies; a positive anomaly in the northwest, another in the Caribbean and a negative anomaly the forms a boundary between the other two (Figure 4.16). As with the 850hPa anomalies, the negative anomaly becomes intense enough to produce anomalous circulations in the northeast. These centers of these anomalies are farther apart than at 850hPa, as the western anomaly is closer to the Pacific Northwest and the eastern anomaly is farther to the northeast. In contrast to the anomalies at 850hPa, negative anomalies extend toward the southwest as far as Texas and northern Mexico.

The location of the positive anomalies during warm phase indicates a more intense ridge in the south-central U.S. that intensifies toward the east. In the north-central U.S., the ridge is weaker during warm phase and becomes indistinguishable from the dominant northeast tilt of the contours (Figure 4.15b). The intensification of the south-central U.S. ridge and the reduction of the geopotential heights to the north intensify the pressure gradient.

During the cold phase of the AMO, the north-central U.S. is under an anomalous anticyclonic circulation. The eastern and south-central U.S. has an anomalous cyclonic circulation anomaly from the low pressure anomaly extending toward the southwest from New England. The reduced ridge and cyclonic wind anomalies during the cold phase of the AMO create fairly extensive positive relative vorticity anomalies throughout much of the south-central and eastern U.S. (Figure 4.17). As relative vorticity can induce baroclinic instability, the increase in positive relative vorticity provides a supportive environment for the initiation and enhancement of disturbances. If compared to Figure 4.1b, there strong similarities between the precipitation and relative vorticity anomalies for each phase of the AMO, indicating the possibility of a casual relationship between the vorticity and precipitation.

The relationship between the circulation and relative vorticity anomalies becomes weaker near Kansas and Nebraska. During the cold phase of the AMO, the circulation anomalies are anticyclonic but there are positive relative vorticity anomalies. A simple bleeding of positive anomalies into the anticyclonic region does not seem to be the cause, as the intrusion is highly localized and does not occur further to the west or east, where similar conditions exist. This suggests that there is another process actively producing increased vorticity in the central U.S. This process would have to be strong enough to counter the negative vorticity produced by anticyclonic circulation anomalies.

Another way to produce relative vorticity anomalies is through the stretching and contraction of an atmospheric vortex. This can occur mechanically by forcing an atmospheric column over a mountain range or dynamically by divergence and

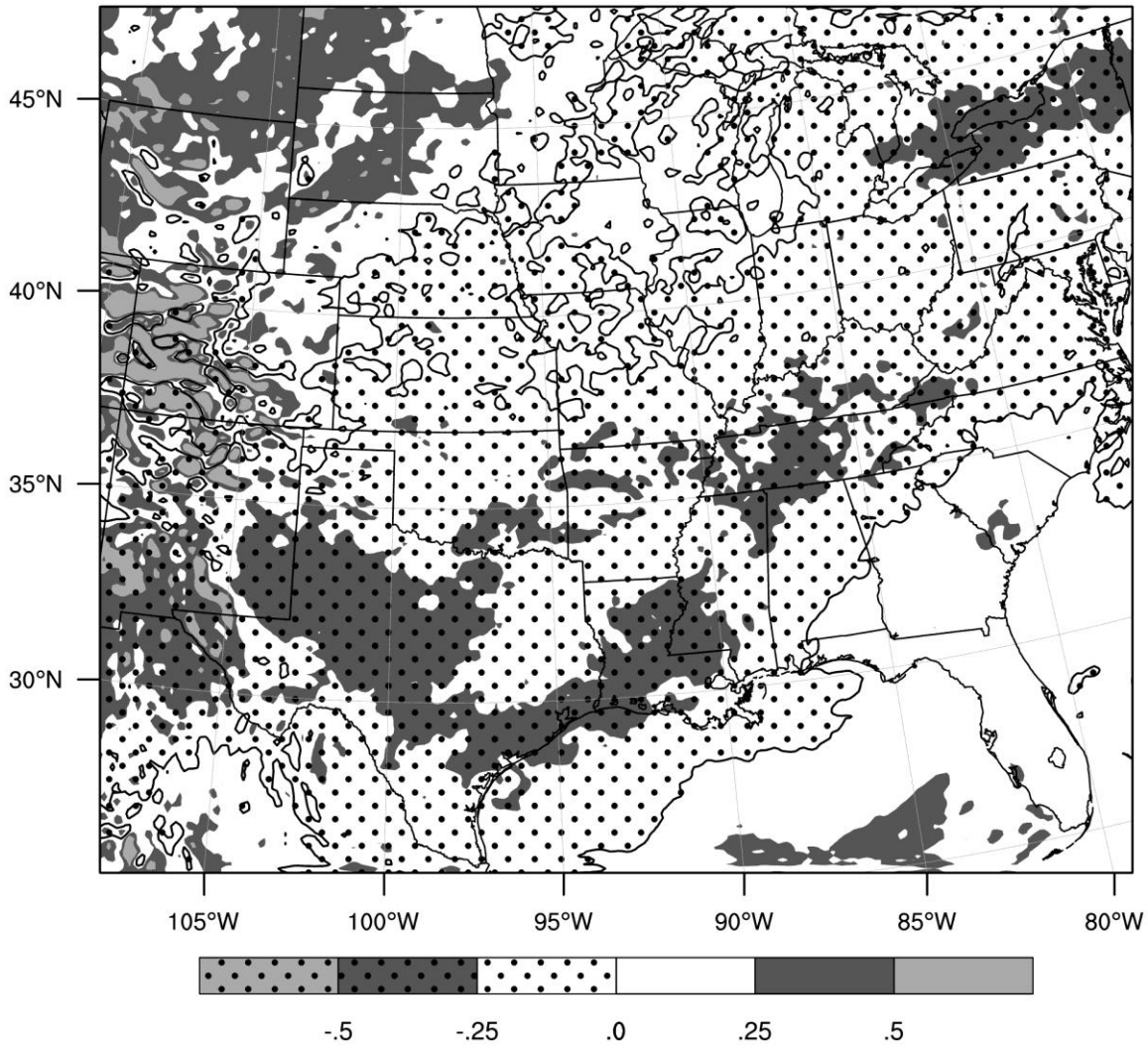

Figure 4.17 JJA 500hPa cold phase relative vorticity anomalies. Units are 10^{-5} s^{-1}. Stippled areas indicate negative values.

convergence (i.e., due to mass conservation). From Holton (2004), we can define the conservation of potential vorticity.

$$(\zeta_\theta + f)\left(-g\frac{\partial\theta}{\partial p}\right) = constant \quad (4)$$

In (4), ζ is relative vorticity, f is planetary vorticity, g is the gravitational constant and $-\partial\theta/\partial p$ is the effective depth of the atmospheric column. For the effective depth, θ is the potential temperature and p is the pressure. Note that pressure is in the denominator. This indicates that when a column stretches (i.e., Δp increases), the effective depth decreases. From the conservation of potential vorticity, we see that if a vortex stretches (i.e., effective depth decreases), then there must be an increase in vorticity. Likewise, a contraction of the atmospheric column would generate a decrease in vorticity. The upper and lower bounds of the column are defined by two potential temperature surfaces.

We can simplify our discussions on the effect of isentropic stretching and contraction if we limit ourselves to a zonal cross-section. Zonal changes in planetary vorticity are zero, thus changes in relative vorticity would vary inversely with effective depth. Figure 4.18 shows the 10-year mean potential temperature anomalies and effective depths along 40°N in the central and eastern U.S. When analyzing the effective depth, it is important to note that it is the way in which the effect depth changes, rather than its absolute value, which determines the generation of vorticity. We can see that in Figure 4.18 that effective depth increases from west to east along 40°N. This indicates that the atmospheric vortex normally contracts and from (4), there should be an increase

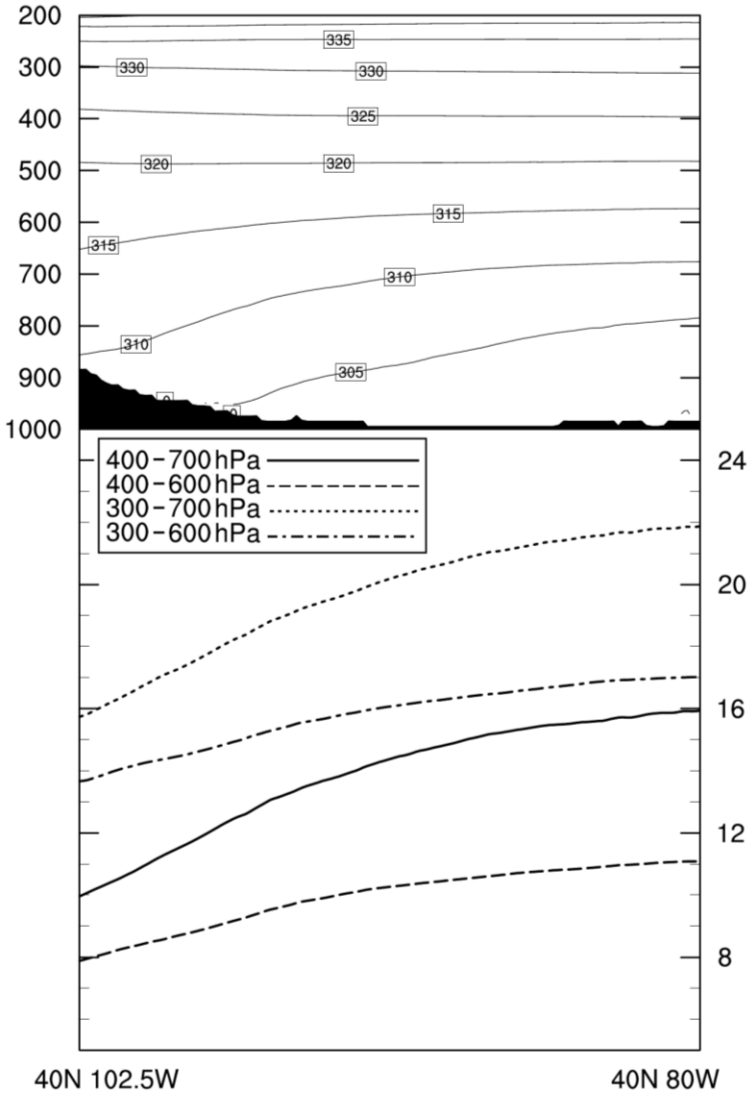

Figure 4.18 JJA average potential temperature cross-section at 40°N (upper panel) and effective depth (lower panel) during the cold phase. Units are K (°C) in the upper panel and K Pa^{-1} in the lower panel. Contour interval in the upper panel is 0.5K.

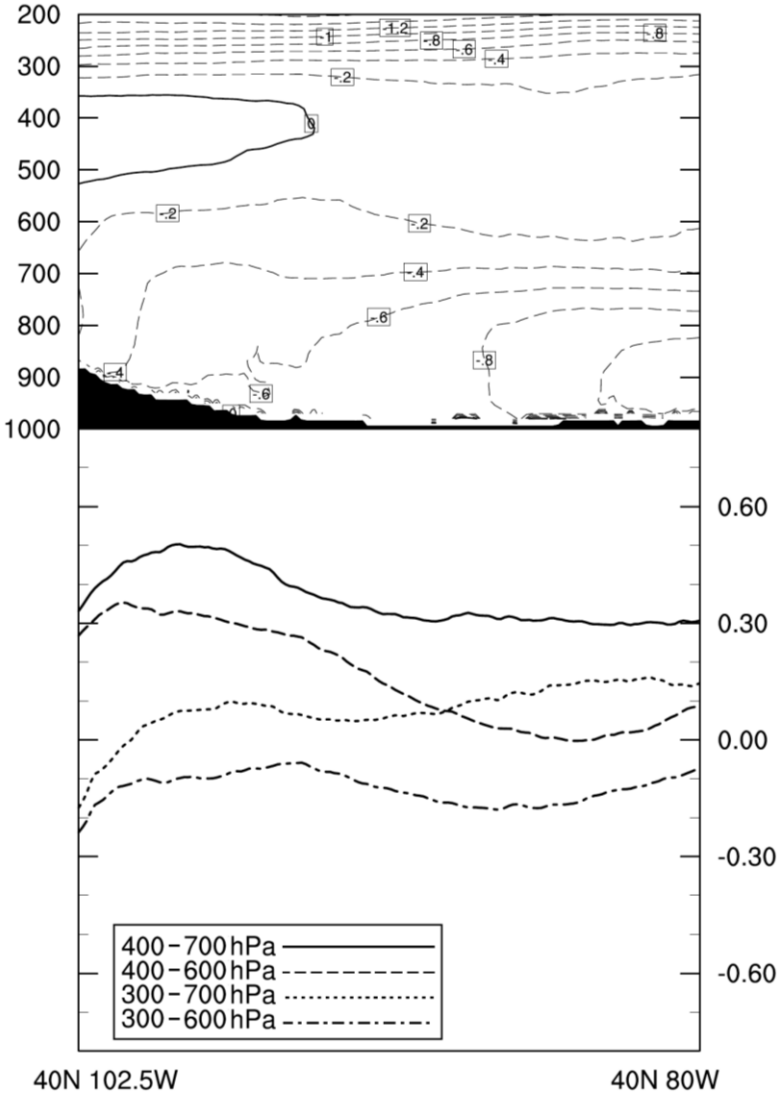

Figure 4.19 JJA cold phase potential temperature anomaly cross-section at 40°N (upper panel) and effective depth (lower panel). Units are K (°C) in the upper panel and K Pa^{-1} in the lower panel. Contour interval in the upper panel is 0.2K. Solid (dashed) lines indicate positive (negative) contours.

in negative relative vorticity. This occurs for all four effective depths presented in Figure 4.18.

Prior to analyzing the effective depth anomalies (Figure 4.19), the meaning of the anomalies should be clarified. A positive anomaly indicates that the atmospheric column has contracted more during that phase of the AMO. Furthermore, a zonal decrease in the effective depth anomalies indicates that the rate of contraction is slower during that phase of the AMO. As previously discussed, the magnitude of the effective depth is unimportant. Rather it is the rate of change that determines the vorticity generation. Thus, to generate positive vorticity anomalies, there needs to be a stretching anomaly. This is produced by a decrease in the effective depth anomalies (i.e., negative slope).

The most striking feature of the potential temperature anomalies during the cold phase of the AMO is the positive anomaly wedge located in the west near 400 to 500hPa. The positive anomalies then weaken toward the east. This indicates that the upper boundary of the conceptual atmospheric column is rising. There does not appear to be a similar process near 600 to 700hPa. This pattern of potential temperature anomalies should decrease the effective depth (and increase vorticity). This is indeed what is found. In the central U.S., the effective depths decrease, most notably between 400 to 600hPa. Slightly further to the east, the lower boundary becomes supportive down to 700hPa. The decrease indicates that, during the cold phase, the rate of contraction is smaller. This results in a smaller amount of negative vorticity generation. In other words, it is a positive vorticity anomaly. An inverse process occurs during the warm phase. The

effective depth increases more rapidly, indicating a more intense production of negative relative vorticity.

The support for the decreased rate of compression of the isentropic surfaces is limited to the mid-troposphere. If the upper boundary for the effective depth calculations is changed to include the potential temperature anomalies at 300hPa, a much weaker or even reverse anomaly pattern emerges. This suggests that the positive relative vorticity generation is limited to 400hPa and below.

Figure 4.20 shows a cross-section of the relative vorticity anomalies along 40°N. During the cold phase of the AMO, the positive relative vorticity anomalies first appear in the west between 400-600hPa. This is consistent with the levels in which stretching anomalies occur (Figure 4.19). Positive vorticity anomalies then appear closer to700hPa. This is also consistent with the effective depth anomalies. This suggests that there is a link between the relative vorticity anomalies and the effective depth anomalies. Further to the east, there are additional (undescribed) processes active to produce the positive vorticity anomalies.

The stretching anomalies of isentropic surfaces are not limited to 40°N. Similar anomalies occur in the central U.S. in zonal cross-sections at 37.5°N and 42.5°N (not shown). Despite the similarities, these areas experience different precipitation anomalies than at 40°N. At 37.5°N, the precipitation anomalies during the cold phase of the AMO are mostly positive (Figure 4.1b). The positive anomalies are weaker or negative at 42.5°N, especially closer toward the Midwest. In some areas, the cross-section at 40°N lies on the boundary between positive and negative anomalies. In other areas, such as

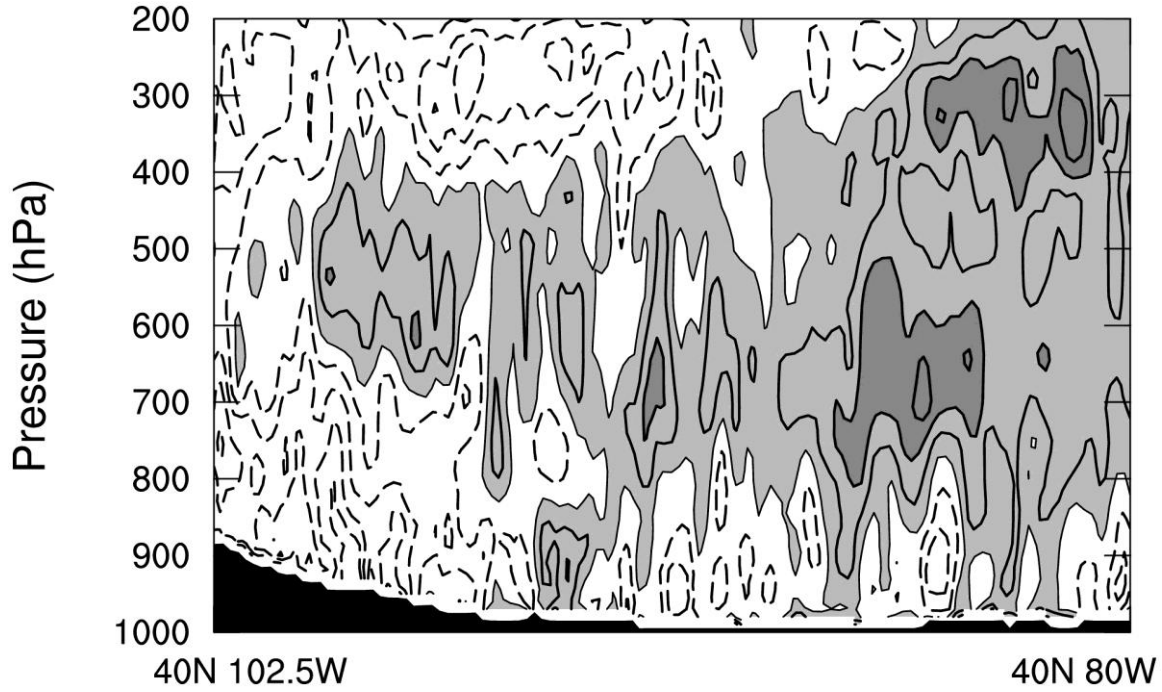

Figure 4.20 JJA cold phase relative vorticity anomalies at 40°N. Units are 10^{-5} s^{-1}. Light shading indicates positive values with moderate shading indicating values greater than 0.2 x 10^{-5} s^{-1}.

Kansas and Nebraska, there are significant positive precipitation anomalies. This variability suggests that the stretching anomalies are not the sole process supporting the precipitation anomalies, but are part of a larger support mechanism in the middle troposphere. The geopotential height anomalies and the resultant circulation anomalies produce positive relative vorticity anomalies in the southern and eastern U.S. In the central U.S. (i.e. Kansas and Nebraska), the stretching anomalies of the isentropic surfaces during the cold phase of the AMO generate sufficient positive relative vorticity anomalies to compensate for the negative relative vorticity induced by the anomalous flow. This allows for the extension to the northwest of the positive relative vorticity anomalies and the increasing precipitation that they help support. Further to the north, the relative vorticity anomalies produced by the stretching anomalies are no longer able to entirely overcome the anomalies produced by the 500hPa circulation anomalies. Thus, the dominance of negative relative vorticity anomalies in the north during the cold phase contributes, through a weakening of the mid-tropospheric support, to the more common negative precipitation anomalies seen in the northern U.S.

The dynamic forcing for the isentropic stretching during the AMO cold phase appears to be mid- to upper-tropospheric convergence (400hPa; Figure 4.21). One implication of the conservation of mass is that a column of air stretches vertically when there is horizontal convergence. Similarly, vertical contraction occurs when there is horizontal divergence. At 500 to 400hPa, there is fairly widespread convergence over the central U.S. (particularly in Kansas and Nebraska). This convergence provides the conditions required for vertical stretching.

The areas of convergence anomalies at 400hPa resemble both the relative vorticity and precipitation anomalies. There is divergence to the north and south of Kansas and Nebraska, but convergence over those two states. This strongly resembles the location of the positive relative vorticity anomalies that cannot be explained by the circulation anomalies, but can be described by the isentropic stretching anomalies. In the north-central U.S., there is no support for increased relative vorticity, either from circulation or convergence anomalies. As shown in Figure 4.2, this area experiences decreased precipitation.

When added to the low-level convergence processes discussed previously, this pattern would seem to inhibit storm development, as there would appear to be convergence throughout the entire atmospheric column The two levels with convergence are actually separated by a fairly thin layer (about 100-150hPa thick) layer of divergence near 700hPa. This thin layer of divergence serves as a boundary between the two layers with mass convergence. In the near-surface layer, there is moisture convergence and then uplift, rising to about 700hPa. This is corresponds with the lower boundary of the dry anomalies discussed in the previous section. At this level, the flow diverges. Above the divergence layer, the convergence produces vertical stretching of the atmosphere, increasing the relative vorticity. The lower boundary of the stretched vortex extends toward 700hPa, providing spin-up for disturbances while tapping into the accumulated low-level moisture and producing an environment more conducive to convective development.

The positive relative vorticity anomalies at 500hPa produced by the circulation anomalies and the isentropic thickness anomalies are critical to the support for positive precipitation anomalies during the cold phase of AMO. Positive relative vorticity is capable of producing the necessary spin-up needed for the development of storm systems. An increase in positive relative vorticity anomalies provides additional support for the formation or intensification of disturbances. When the mid-tropospheric processes are combined with the increase in moisture near the surface and a more convectively unstable atmospheric profile, there is strong support for the increases in precipitation that are seen in the central U.S.

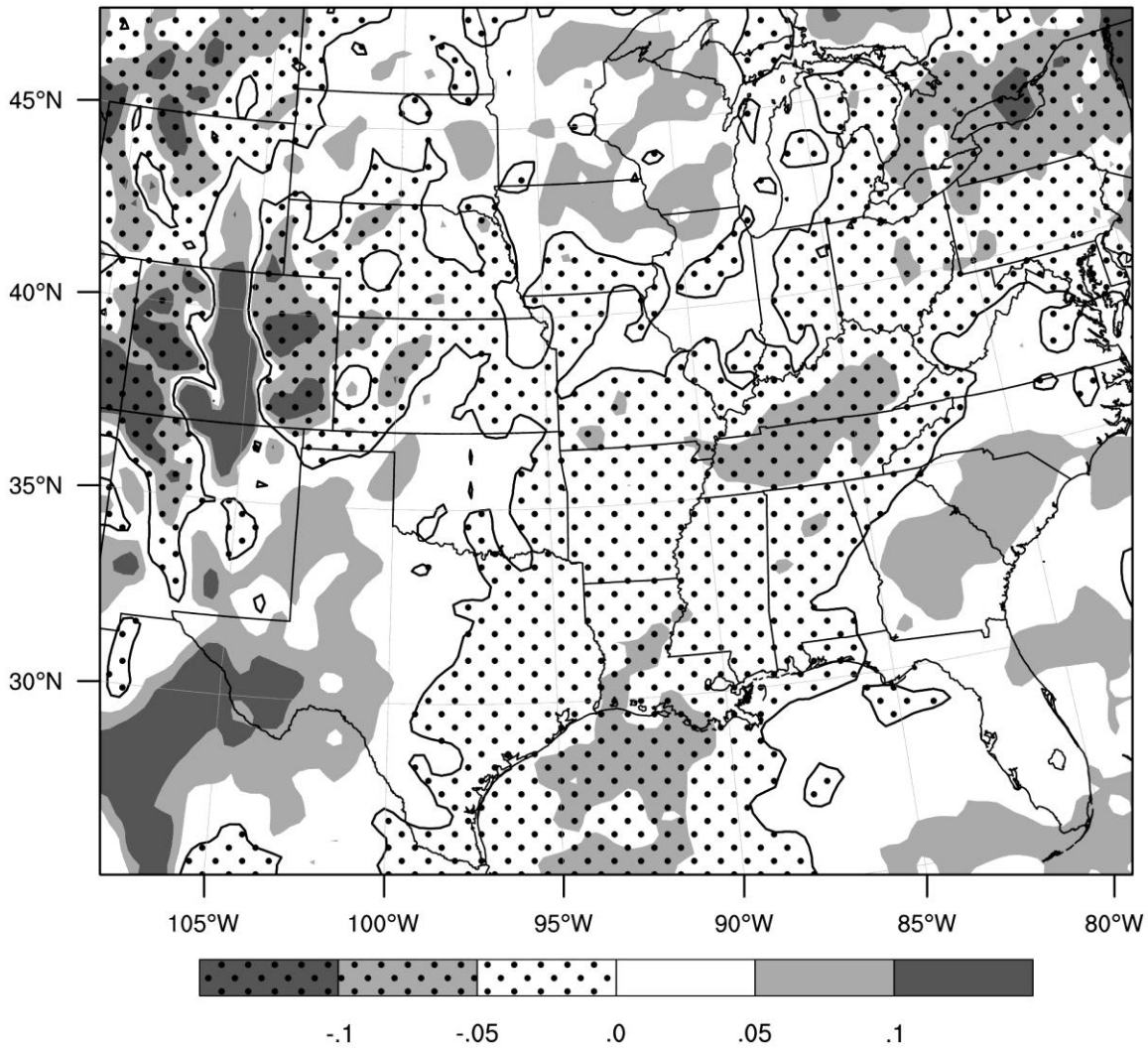

Figure 4.21 JJA 400hPa divergence anomalies for the cold phase from the AMO-forced WRF simulations. Stippled areas indicate negative values. Units are 10^{-5} s^{-1}.

Chapter 5

Summary and Future Work

5.1 Summary

This study provides a better understanding of how the Atlantic Multidecadal Oscillation (AMO) influences summer (JJA) precipitation over the central U.S. and how this influence is achieved at region scales. To do this, the Weather Research and Forecasting (WRF) regional model was used to resolve the regional-scale processes.

The WRF simulations driven by the AMO-forced GCM results from Hu et al. (2011) revealed a set of complex processes by which the AMO influences summer precipitation over North America, especially the central U.S. In the lower troposphere (below 700hPa), the major contributor to precipitation anomalies in the central U.S. is the anomalies in the geopotential heights and moisture. The geopotential height anomalies directly influence the low level wind fields and in turn, the moisture distribution and convergence.

The large-scale anomalies in the geopotential heights are determined by the expansion of the North Atlantic Subtropical High Pressure (NASH). During the AMO cold phase, NASH extends over the continental U.S. and increases the low-level geopotential heights. Locally over the central U.S., there is a greater increase in heights in the north-central U.S. than elsewhere. This anomaly pattern reduces the pressure gradient force in the central U.S. and as a result of this; there is a reduction in the moist low-level jet (LLJ). The LLJ decrease is greatest to the north, producing a southerly flow

that slowly weakens to the north (relative to the warm phase) and creates a moisture convergence anomaly that pools moisture in the central U.S.

Another result of the low-level circulation anomalies is that there is a decrease in the atmospheric moisture above 700hPa. Above this level, the flow is more westerly during the cold phase of the AMO. This weakens the connection to the moist flow from the Gulf of Mexico and the flow originates from closer to the southwestern U.S. and northern Mexico. The presence of drier air overlying the more moist air near the surface produces a more convectively unstable atmosphere.

A favorable mid-tropospheric dynamic background is able to utilize the potential instability produced by the moisture anomalies. At 500hPa, much of the central U.S. has increased relative vorticity during the cold phase of the AMO. Increased vorticity allows for greater spin-up of atmospheric disturbances and baroclinic instability.

The increased relative vorticity during the cold phase appears to be from two processes. In the south-central and eastern U.S., the increase occurs in conjunction with cyclonic circulation anomalies. These circulation anomalies are likely the source of at least most of the relative vorticity increase. Near Kansas and Nebraska, positive relative vorticity anomalies occur that agree well with the precipitation anomalies, but occur in an area with anticyclonic circulation anomalies. It was found that anomalous vertical stretching of the atmosphere can account for the increased relative vorticity. The stretching anomaly first occurs in the western Great Plains between 400 to 600hPa. Slightly to the east, the stretching descends to 700hPa. This agrees well with the relative vorticity anomalies along 40°N. A source of the stretching appears to be convergence in

the mid- to upper troposphere. Horizontal convergence forces vertical stretching and induces an increase in relative vorticity. The increased relative vorticity advects down toward 700hPa, where thin level of divergence separates the upper- and lower-level convergence. At this level, the positive relative vorticity anomalies contribute to the spin-up of disturbances and break through the boundary between the increased low-level moisture and decreased mid-level moisture. This allows for the utilization of the increased convective instability and produces the increased precipitation during the cold phase of the AMO.

At their core, the mechanisms proposed in this research are primarily dependent on regional-scale variations in the large-scale processes. It is regional variations in low-level pressure that produce the moisture convergence anomalies. A relatively small area of convergence at and above 500hPa appears to be responsible for the atmospheric stretching anomalies. The stretching anomalies occur over the most statistically significant precipitation anomalies in the central U.S. (i.e., Kansas and Nebraska). These examples show that regional-scale processes do seem to be important in determining the AMO-forced precipitation anomalies.

Finally, a better understanding of the regional processes forced by the AMO allows for better forecasting of precipitation in the central U.S. The identification of the mechanism presented in this research could allow for the mitigation of the resultant precipitation anomalies. This can potentially provide advance notice to municipalities to be alert for potentially disruptive precipitation anomalies and floods.

5.2 Future Work

While this study is able to provide a viable mechanism for how the AMO is able to influence regional circulation and summer precipitation anomalies in the central U.S., there are several potential ways to strengthen and expand this work. The first of which would be an expansion of the number of years used in the study. It was shown in chapter 3 that the dynamics of the ten years chosen for the validation do not entirely agree with the average fields for an entire cycle of the AMO. As the same methodology was used in selecting the years from both the Reanalysis and the AMO-forced GCM data, it can be argued that the AMO-forced data could contain similar discrepancies. Since the AMO-forced GCM data are, by definition, only forced by the AMO, this would suggest a reduced probability for similar discrepancies, but the very nature of model internal variability would suggest that inconsistencies between the selected years and the full range of data could be a potential issue that could be explored further. Expanding the number of years used by at least two to three times the number used in this study should provide a stronger dataset to verify (or modify) these findings.

Another potential direction for furthering this research would be in expanding the modeled period into September and examining the monthly variability between all of the months in the warm season. This study was interested in the summer (JJA) precipitation in the central U.S., but there were indications that there is some variability between early and late summer (i.e., June and August). There were preliminary results that suggested that there may be some intra-seasonal variability in the mechanism that controls the AMO-forced precipitation anomalies. By examining the monthly anomalies and

extending the simulations into September, it could be explored whether there are significant variations within the summer. It could also be possible to determine whether some processes occur prior to others and if so, perform autocorrelations to determine any temporal relationships between the processes. Any significant lags could potentially be used to improve the forecasting of AMO-forced precipitation anomalies, as it could potentially allow for early identification of AMO-forced processes.

This research can also be supplemented by the use of a simplified vorticity model. A major component of the mechanism proposed in this research is the positive relative vorticity anomalies produced during the cold phase due to a reduced amount of isentropic compression over the central U.S. Circulation and isentropic stretching anomalies are two significant ways in which relative vorticity can change between the two phases of the AMO. It was shown that the model indicated that there were positive relative vorticity anomalies at 500hPa over the central U.S. in areas with anticyclonic rotation anomalies. It was inferred that the reduced isentropic contraction that occurs during the cold phase would be enough to reverse the anomalies to what was shown at 500hPa. A simplified vorticity model could be used to determine whether this is actually the case. The regional model is able to produce high resolution (both temporal and spatial) data about the isentropic surfaces and how they change. Using these data to force a vorticity model would determine the vorticity anomalies induced by the changes in the isentropic surfaces between the two phases of the AMO.

As this research is presented primarily as qualitative results, the use of a simplified vorticity model would introduce more quantitative aspect to this study. A

more quantitative approach can be used in other areas to expand upon what has been presented in this research. With a greater sample size (i.e. more years), a stronger statistical analysis could be performed in order to verify the connection between the proposed mechanism and the precipitation anomalies.

This study can also be expanded to include forcings beyond the AMO. The inclusion of ENSO or PDO forcings in addition to the AMO would allow for investigation as to the importance of these processes described in this study in relation to real-world conditions. The results could be compared to GCM simulations with similar forcings (e.g., Mo et al. 2009; Hu et al. 2011) to determine whether there are any regional-scale processes that occur with either ENSO, PDO forcing or a combination of these forcings with the AMO.

Any of the possibilities presented in this section can potentially improve our understanding of precipitation variations in the central U.S. Extending the simulations into September and examining the variations within the summer would be the easiest to perform. Expanding the forcings to include either ENSO or PDO would be the next simplest, as this study would serve as a template for examining the results. The most complicated of these potential studies would be the simplified vorticity model, as it would be a fairly large departure from the model and methods used in this study. Regardless of complexity, any of these ideas can potentially extend our understanding of precipitation variations in the central U.S.

References

Anderson, C. J., and R. W. Arritt, 1998: Mesoscale Convective complexes and persistent elongated convective systems over the United States during 1992 and 1993. *Mon. Wea. Rev.*, **126**, 578–599.

Arritt, R. W., T. D. Rink, M. Segal, D. P. Todey, C. A. Clark, M. J. Mitchell, and K. M. Labas, 1997: The Great Plains low-level jet during the warm season of 1993. *Mon. Wea. Rev.,* **125**, 2176-2192.

Beck, C., J. Grieser and B. Rudolf, 2005: A new monthly precipitation climatology for the global land areas for the period 1951 to 2000. DWD, Klimastatusbericht KSB 2004, ISSN 1437-7691, ISSN 1616-5063 (Internet), ISBN 3-88148-402-7, 181-190.

Bell, G. D., and J. E. Janowiak, 1995: Atmospheric circulation associated with the Midwest floods of 1993. *Bull. Am. Meteorol. Soc.,* **76**, 681-695.

Bonner, W., 1968: Climatology of the low level jet, *Mon. Weather Rev.*, **96**, 833-850.

Delworth, T., S. Manabe, and R. J. Stouffer, 1993: Interdecadal variations of the thermohaline circulation in a coupled ocean-atmosphere model. *J. Clim.*, **6**, 1993-2011.

Enfield, D. B., A. M. Mestas-Nunez, and P. J. Trimble, 2001: The Atlantic multidecadal oscillation and its relation to rainfall and river flows in the continental US. *Geophys. Res. Lett.,* **28**, 2077-2080.

Feng, S., R. J. Oglesby, C. M. Rowe, D. B. Loope, and Q. Hu, 2008: Atlantic and Pacific SST influences on Medieval drought in North America simulated by the Community Atmospheric Model. *J. Geophys. Res.-Atmos.,* **113**, D11101, doi:10.1029/2007JD009347.

Feng, S., Q. Hu and R.J. Oglesby, 2010: Influence of Atlantic sea surface temperature on persistent drought in North America. *Climate Dynamics*, DOI 10.1007/s00382-010-0835-602x

Gray, S. T., L. J. Graumlich, J. L. Betancourt, and G. T. Pederson, 2004: A tree-ring based reconstruction of the Atlantic Multidecadal Oscillation since 1567 AD. *Geophys. Res. Lett.,* **31**, L12205, doi:10.1029/2004GL019932.

Guan, B., and S. Nigam, 2009: Analysis of Atlantic SST variability factoring interbasin links and the secular trend: clarified structure of the Atlantic Multidecadal Oscillation. *J. Clim.,* **22**, 4228-4240, doi:10.1175/2009JCLI2921.1.

Higgins, R. W., Y. Yao, E. S. Yarosh, J. E. Janowiak, and K. C. Mo, 1997: Influence of the Great Plains low-level jet on summertime precipitation and moisture transport over the central United States. *J.Clim.,* **10**, 481-507.

Holton, J. R., 2004: *An introduction to dynamic meteorology.* 4th ed. International geophysics series, Vol. 88, Elsevier Academic Press, 535 pp.

Hu, Q., and S. Feng, 2007: Decadal variation of the southwest US summer monsoon circulation and rainfall in a regional model. *J. Clim.,* **20**, 4702-4716.

Hu, Q., and S. Feng, 2008: Variation of the North American summer monsoon regimes and the Atlantic multidecadal oscillation. *J. Clim.,* **21**, 2371-2383.

Hu, Q., S. Feng, R. Oglesby, 2011: Variations in North American summer precipitation driven by the Atlantic Multidecadal Oscillation. *J. Clim.* (in press)

Kalnay, E., M. Kanamitsu, R. Kistler, W. Collins, D. Deaven, L. Gandin, M. Iredell, S. Saha, G. White, J. Woollen, Y. Zhu, M. Chelliah, W. Ebisuzaki, W. Higgins, J. Janowiak, K.C. Mo, C. Ropelewski, J. Wang, A. Leetmaa, R. Reynolds, R. Jenne, and D. Joseph, 1996: The NCEP/NCAR 40-year reanalysis project. *Bull. Amer. Meteor. Soc.*, **77**, 437-471.

Kerr, R. A., 2000: A North Atlantic climate pacemaker for the centuries. *Science,* **288**, 1984-1986.

Kistler, R., E. Kalnay, W. Collins, S. Saha, G. White, J. Woollen, M. Chelliah, W. Ebisuzaki, M. Kanamitsu, V. Kousky, H. van den Dool, R. Jenne, and M. Fiorino, 2001: The NCEP-NCAR 50-Year Reanalysis: Monthly Means CD-ROM and Documentation. *Bull. Amer. Meteor. Soc.*, **82**, 247-267.

Knight, J. R., R. J. Allan, C. K. Folland, M. Vellinga, and M. E. Mann, 2005: A signature of persistent natural thermohaline circulation cycles in observed climate. *Geophys. Res. Lett.,* **32**, L20708, doi:10.1029/2005GL024233.

Latif, M., E. Roeckner, M. Botzet, M. Esch, H. Haak, S. Hagemann, J. Jungclaus, S. Legutke, S. Marsland, U. Mikolajewicz, and J. Mitchell, 2004: Reconstructing, monitoring, and predicting multidecadal-scale changes in the North Atlantic thermohaline circulation with sea surface temperature. *J. Clim.,* **17**, 1605-1614.

McCabe, G. J., M. A. Palecki, and J. L. Betancourt, 2004: Pacific and Atlantic Ocean influences on multidecadal drought frequency in the United States. *Proc. Natl. Acad. Sci. U.S.A.,* **101**, 4136-4141, doi:10.1073/pnas.0306738101.

Mo, K. C., J. N. Paegle, and R. W. Higgins, 1997: Atmospheric processes associated with summer floods and droughts in the central United States. *J. Clim.,* **10**, 3028-3046.

Mo, K. C., J. E. Schemm, and S. Yoo, 2009: Influence of ENSO and the Atlantic Multidecadal Oscillation on Drought over the United States. *J. Clim.,* **22**, 5962-5982, doi:10.1175/2009JCLI2966.1.

Namias, J., 1983: Some causes of United States drought. *J. Climate Appl. Meteor.*, **22**, 30–39.

Oglesby, R. J., and D. J. Erickson III, 1989: Soil moisture and the persistence of North American drought, *J. Clim.*, **2**, 1362-1380.

Rasmusson, E. M., 1967: Atmospheric water vapor transport and water balance of North America .I. Characteristics of water vapor flux field. *Mon. Weather Rev.*, **95**, 403-426, doi:10.1175/1520-0493.

Rudolf, B., C. Beck, J. Grieser, U. Schneider, 2005: Global precipitation analysis products. Global Precipitation Climatology Centre (GPCC), DWD, Internet publication, 1-8.

Rudolf, B., T. Fuchs, U. Schneider and A. Meyer-Christoffer, 2003: Introduction of the Global Precipitation Climatology Centre (GPCC), Deutscher Wetterdienst, Offenbach a.M.; 16 pp.

Rudolf, B., and U. Schneider, 2005: Calculation of Gridded Precipitation Data for the Global Land-Surface using in-situ Gauge Observations, Proceedings of the 2nd Workshop of the International Precipitation Working Group IPWG, Monterey October 2004, EUMETSAT, ISBN 92-9110-070-6, ISSN 1727-432X, 231-247.

Ruiz-Barradas, A., S. Nigam, 2005: Warm season rainfall variability over the US Great Plains in observations, NCEP and ERA-40 reanalyses, and NCAR and NASA atmospheric model simulations. *J. Clim.*, **18**, 1808-1830.

Skamarock, W. C., J. B. Klemp, J. Dudhia, D. O. Gill, D. M. Barker, W. Wang, and J. G. Powers, 2005: A description of the Advanced Research WRF Version 2. NCAR Tech Notes-468+STR

Schubert, S. D., M. J. Suarez, P. J. Pegion, R. D. Koster, and J. T. Bacmeister, 2004: On the cause of the 1930s Dust Bowl. *Science,* **303**, 1855-1859.

Sutton, R. T., and D. L. R. Hodson, 2005: Atlantic Ocean forcing of North American and European summer climate. *Science,* **309**, 115-118, doi:10.1126/science.1109496.

Ting, M. F., and H. Wang, 1997: Summertime US precipitation variability and its relation to Pacific sea surface temperature. *J. Clim.*, **10**, 1853-1873.

Trenberth, K. E., and C. J. Guillemot, 1996: Physical processes involved in the 1988 drought and 1993 floods in North America. *J. Clim.,* **9**, 1288-1298.

Tuttle, J. D., and C. A. Davis, 2006: Corridors of warm season precipitation in the central United States. *Mon. Wea. Rev.*, **134**, 2297-2317.

Wang, C., S. Lee, and D. B. Enfield, 2007: Impact of the Atlantic warm pool on the summer climate of the Western Hemisphere. *J. Clim.,* **20**, 5021-5040, doi:10.1175/JCLI4304.1.

Wang, C., S. Lee, and D. B. Enfield, 2008: Climate response to anomalously large and small Atlantic warm pools during the summer. *J. Clim.*, **21**, 2437-2450, doi:10.1175/2007JCLI2029.1.

Wang, H., S. Schubert, M. Suarez, and R. Koster, 2010: The physical mechanisms by which the leading patterns of SST variability impact US precipitation. *J. Clim.*, **23**, 1815-1836, doi:10.1175/2009JCLI3188.1.